Transient Permeation of Butanes through ZSM-5 and ZSM-11 Zeolite Membranes

Tracy Q. Gardner, John L. Falconer, and Richard D. Noble
Dept. of Chemical Engineering, University of Colorado, Boulder, CO 80309-0424

DOI 10.1002/aic.10217
Published online in Wiley InterScience (www.interscience.wiley.com).

Butane isomer adsorption isotherms and diffusivities in the transport pathways through Al-ZSM-11 (MEL), Al-ZSM-5 (MFI), and B-ZSM-5 zeolite membranes were measured by a transient permeation technique. The permeate responses to feed step changes were measured between 383 and 473 K, and the diffusion was modeled as Maxwell–Stefan surface diffusion with dual-site Langmuir adsorption. The effects of adsorption and diffusion on the n-C_4/i-C_4 ideal selectivities were quantified, and the selectivity differences between the membranes were explained based on the adsorption properties and the diffusivities. The resistance of the porous tubular supports affected the coverage in the zeolite at the permeate boundary, and the ratio of the n-C_4/i-C_4 diffusion driving forces consequently increased with increasing temperature. The n-C_4 diffusivities were almost the same in the three membranes, but the i-C_4 diffusivities in the MEL membrane were an order of magnitude higher than those in the MFI membranes. The bulkier i-C_4 molecules are apparently significantly less constrained in the straight, circular pores and slightly larger intersections of MEL zeolite, although the structural differences do not affect the mobility of n-C_4. Higher i-C_4 coverages in the Al-ZSM-11 and B-ZSM-5 membranes compared to the Al-ZSM-5 membrane were attributed to a smaller change in entropy upon adsorption in the channels of Al-ZSM-11 and to a higher heat of adsorption in the intersections of the more substituted B-ZSM-5. Initial transient flux overshoots and undershoots after i-C_4 feed concentration changes were apparently caused by a small amount of pressure-driven flow ($<10\%$ of the total i-C_4 flux and $<0.1\%$ of the total n-C_4 flux) through parallel pathways. The effective membrane thicknesses were also estimated from the transient measurements. *AIChE J,* 50: 2816–2834, 2004
Keywords: ZSM-11 (MEL) zeolite; B-ZSM-5 (MFI) zeolite; membrane adsorption; Maxwell–Stefan diffusion; transient permeation

Introduction

Zeolite membranes are polycrystalline films that are grown on porous supports to provide mechanical stability. Because their pore sizes are of molecular dimensions and they have high chemical and thermal stability, zeolite membranes have the potential to perform many industrially important separations. Films of zeolite types MFI (Bai et al., 1995; Bakker et al., 1996; Bein, 1996; Davis and Lobo, 1992; den Exter et al., 1996; Gora et al., 2001; Jia et al., 1994; Kapteijn et al., 1995a; Matsukata et al., 1993; Noble and Falconer, 1995; Tuan et al., 1999; Vroon, 1995; Vroon et al., 1998; Xomeritakis et al., 1999; Yan et al., 1995), FER (Matsukata et al., 1996; Nishiyama et al., 1997), FAU (Bein, 1996; Kusakabe et al., 1998, 1999; Li et al., 2001), LTA (Bein, 1996; Hedlund et al., 1997; Matsukata and Kikuchi, 1997), MOR (Bein, 1996; Matsukata

Correspondence concerning this article should be addressed to J. L. Falconer at john.falconer@colorado.edu.

and Kikuchi, 1997), MEL (Tuan et al., 2001), ANA (Matsukata and Kikuchi, 1997), AFI (Bein, 1996), Beta (Tuan et al., 2002), and zeolite L (Bein, 1996) have been reported, with silicalite and ZSM-5 (both MFI-type) receiving the most attention.

In the [010] direction, the MFI zeolite structure has straight-through, nearly circular pores of 10-membered rings (for example, in silicalite-1, 10 silicons bound in a ring by oxygen bridges, where the 10 oxygen atoms form the pore window) that are approximately 0.53×0.56 nm in diameter. Sinusoidal elliptical pores of 10-membered rings that are about 0.51×0.57 nm in diameter run in the [100] direction. These pore sizes were determined from XRD measurements, but the zeolite framework is flexible so molecules with kinetic diameters larger than these dimensions can fit in the pores (van Koningsveld and Jansen, 1996). The straight and sinusoidal pores intersect to make supercages, the centers of which are separated by approximately 1 nm (Meier and Olson, 1992). Heats and entropies of adsorption are different in the channels and intersections of this structure, and depending on the temperature and the adsorbate, molecules fill either the channels or intersections first (Vlugt et al., 1999; Zhu et al., 2000).

Zeolite ZSM-5 has the MFI structure with some of the Si atoms replaced by other atoms such as aluminum, boron, germanium, and iron to improve catalytic or membrane properties (Tuan et al., 2000a,b). When the substituted cation has a valence other than +4, the framework has a net charge that must be balanced by associated ions that are not part of the framework, but sit in the channels or intersections near the substituted atom. Aluminum has been the atom most often substituted into the zeolite framework of the MFI structure. Unless otherwise mentioned, the associated cation in the zeolites used in the current study is H^+.

Boron-substituted ZSM-5 membranes have shown good separation behavior for butane isomers at high temperatures (Tuan et al., 2000b). Molecular transport through zeolite membranes occurs by surface diffusion; molecules adsorb onto the zeolite from a gas or liquid phase at one side, diffuse as separate molecules from adsorption site to adsorption site in the zeolite structure, and desorb into the permeate stream. Thus, the higher selectivities in B-ZSM-5 membranes could be attributable to larger adsorption and/or larger diffusion differences between the two molecules in B-ZSM-5 than in Al-ZSM-5.

The MEL structure is similar to the MFI structure except that both types of channels are straight. In MEL the channels in both directions are about 5.3×5.4 nm. Supported B-ZSM-11 membranes, recently prepared in our laboratory, separated MEK/water (Tuan et al., 2001) and alcohol/water mixtures (Li et al., 2002) by pervaporation. The alcohol/water separation selectivities for linear C_1–C_3 alcohols were higher than those obtained by vapor–liquid equilibrium. The separation selectivities were attributed to both differences in diffusion rates and preferential adsorption; mixture selectivities were higher than ideal selectivities (Li et al., 2002).

Intracrystalline surface diffusion generally dominates transport through high-quality zeolite membranes. The Maxwell–Stefan diffusion model, accounting for the interactions between diffusing molecules and their interactions with the zeolite surface, has been shown to quantitatively describe steady-state and transient diffusion in zeolites and zeolite membranes (Bakker et al., 1996; Burggraaf, 1999; Gardner et al., 2002a; Kapteijn et al., 1995b, 2000; Krishna and van den Broeke, 1995; van den Broeke, 1994). The thermodynamic correction factor used in the Maxwell–Stefan diffusion model is calculated from the adsorption model. Zhu et al. (1998) measured adsorption isotherms of butane isomers in silicalite powders with a tapered element oscillating microbalance (TEOM). Langmuir type I adsorption well described n-C_4 and i-C_4 adsorption at temperatures of 383 K and above. At lower temperatures a dual-site Langmuir isotherm, treating the channels and intersections as adsorption sites with different sorption capacities and adsorption equilibrium constants, was necessary to describe the behavior of i-C_4. These results agreed with molecular simulations (Goodbody et al., 1991; Vlugt et al., 1999) that showed that linear alkanes preferentially adsorb in the silicalite channels, but also adsorb in the intersections at high coverages. These simulations also showed that branched alkanes preferentially reside in the channel intersections, and at higher coverage they also adsorb into the channels. Zhu et al. (2000) reconciled TEOM adsorption isotherm measurements of butane isomers with molecular simulations by applying a dual-site Langmuir adsorption model for all conditions. The experiments and the simulations agreed and indicated that eight n-C_4 molecules/unit cell first adsorb in the silicalite channels, and at higher pressures two more molecules/unit cell adsorb in the intersections. At lower pressures i-C_4 first fills four intersection sites/unit cell and at higher pressures it fills six channel sites/unit cell. Molecular simulations showed that i-C_4 first fills 4 intersection sites/unit cell for a MEL zeolite also and six more sites/unit cell at higher pressures (Maesen et al., 2001; Schenk et al., 2002).

We recently developed a transient permeation method that measures adsorption isotherms for the transport pathways through zeolite membranes and simultaneously determines diffusivities and effective membrane thickness. The transient permeate responses to feed step changes were measured and modeled as Maxwell–Stefan diffusion with Langmuir type I adsorption. Isotherms and thermodynamic properties generated by this method at 295 K for N_2, CH_4, and CO_2 (Gardner et al., 2002a) and from 295 to 473 K for butane isomers (Gardner et al., 2002b) in high-quality H-ZSM-5 membranes were remarkably similar to those obtained by calorimetry and uptake measurements for MFI crystals. This suggested that these gases permeated mainly through zeolite pores, and it also indicated that the transient method was valid for characterizing membrane properties when most of the flow was through zeolite pores. When the transient responses of butane isomers were analyzed, the support resistance had to be included in the model to obtain reasonable thermodynamic parameters.

In the current study, the transient model was extended to include dual-site Langmuir adsorption. Diffusivities and adsorption isotherms of butane isomers were measured at 373–473 K in Al-ZSM-5, Al-ZSM-11, and B-ZSM-5 membranes. The differences in ideal selectivities of the three membranes and their temperature dependencies are explained quantitatively based on the heats and entropies of adsorption and activation energies for diffusion.

Theory

The transient permeation method for measuring adsorption in membranes has been described in detail previously (Gardner et al., 2002a,b, 2003). This method is based on relating the

amount adsorbed at steady state, Q_c, as calculated from the integrated, steady-state coverage profile, $q_{SS}(z)$

$$Q_c = \rho A \int_0^{\delta} q_{SS}(z)dz \tag{1}$$

(ρ = zeolite density, A = permeation area, δ = membrane thickness) to the amount adsorbed during the transient response to a feed step change, Q_t, as measured from the integrated difference between the transient fluxes (J) into and out of the membrane

$$Q_t = A \int_0^{\infty} (J_{in} - J_{out})dt = (n_{SS} - n_i) \tag{2}$$

(n_{SS} = total moles in membrane at steady state, which is also equal to Q_c; n_i = total moles in membrane before step change at $t = 0$).

Transient model

The transport through the membranes was modeled as Maxwell–Stefan surface diffusion, which results in the following transient occupancies

$$\frac{\partial \theta}{\partial t} = Đ_{MS} \frac{\partial}{\partial z}\left(\Gamma \frac{\partial \theta}{\partial z}\right) \tag{3}$$

where $Đ_{MS}$ is the Maxwell–Stefan diffusivity, θ is the fractional occupancy in the zeolite pores, and Γ is a thermodynamic correction factor

$$\Gamma = \frac{q}{P}\frac{\partial P}{\partial q} \tag{4}$$

describing the occupancy dependency of the diffusivity ($D = Đ_{MS}\Gamma$). The thermodynamic factor is determined from the adsorption isotherm, and arises because the driving force for diffusion through zeolite membranes is the chemical potential gradient rather than the pressure gradient.

Adsorption was modeled using single-site and dual-site Langmuir isotherms for comparison. For single-site isotherm analysis, the coverage is

$$\theta = \frac{q}{q_{sat}} = \frac{bP}{1 + bP} \tag{5}$$

(q_{sat} = saturation coverage, b = adsorption equilibrium constant, P = partial pressure of permeant), and the parameters determined for each feed partial pressure were q_{sat} and b. For dual-site Langmuir isotherm analysis, the coverage is

$$\theta = \frac{q}{q_{sat,tot}} = \frac{f_C b_C P}{1 + b_C P} + \frac{f_I b_I P}{1 + b_I P} \tag{6}$$

In the dual-site analysis the subscripts C and I indicate channel and intersection sites, respectively; $q_{sat,tot}$ is the total saturation coverage ($q_{satC} + q_{satI}$); and f_i is the fractional coverage of site i at saturation ($f_C = q_{satC}/q_{sat,tot}$). The transient data were analyzed assuming q_{satC} = 8 and 6 and q_{satI} = 2 and 4 molecules/unit cell (molec./u.c.) for n-C_4 and i-C_4, respectively. The adsorption equilibrium constants for the two sites (b_C and b_I) were determined from the analysis of the transients. Note that the same saturation values are used for both MEL and MFI membranes because molecular simulations indicated the q_{sat} values were the same for the two structures (Schenk et al., 2002).

Adsorption

For single-site adsorption, the steady-state coverage profile was obtained by solving Eq. 3 at steady state with boundary conditions q_0 and q_d calculated from the feed and permeate side partial pressures. The support resistance was included in the model in the determination of P_δ, as described previously (Gardner et al., 2002b). The coverage profile was subsequently integrated (Eq. 1) over the thickness of the membrane, δ, to obtain Q_c

$$Q_c = \rho A q_{sat}\delta\left[1 + \frac{\dfrac{q_0 - q_\delta}{q_{sat}}}{\ln\left(\dfrac{q_{sat} - q_0}{q_{sat} - q_\delta}\right)}\right] \tag{7}$$

For dual-site adsorption, we were not able to solve for $q_{SS}(z)$, but the integrated, steady-state coverage profile was calculated from $q_{SS}(P)$ instead by

$$Q_c = \rho A \int_0^{\delta} q_{SS}(z)dz = \rho A \int_{P_0}^{P_\delta} q_{SS}(P)\frac{dz}{dP}\,dP \tag{8}$$

The relationship between P and z was determined by integrating Eq. 3, written in terms of pressure, twice over z with $P = P_0$ and $P = P_\delta$ boundary conditions and solving for z

$$\frac{z}{\delta} = \frac{q_{satA}\ln\left(\dfrac{1 + b_I P_0}{1 + b_I P}\right) + q_{satB}\ln\left(\dfrac{1 + b_C P_0}{1 + b_C P}\right)}{q_{satA}\ln\left(\dfrac{1 + b_I P_0}{1 + b_I P_\delta}\right) + q_{satB}\ln\left(\dfrac{1 + b_C P_0}{1 + b_C P_\delta}\right)} \tag{9}$$

Taking the derivative of $z(P)$ with respect to P and substituting the result into Eq. 8 yields the expression for Q_c for dual-site adsorption

$$Q_c = \rho A q_{sat,tot}\delta \times \left[\frac{C1(P_0 - P_\delta) + C2\,\ln\left(\dfrac{1 + b_C P_\delta}{1 + b_C P_0}\right) + C3\,\ln\left(\dfrac{1 + b_I P_\delta}{1 + b_I P_0}\right)}{f_C \ln\left(\dfrac{1 + b_C P_\delta}{1 + b_C P_0}\right) + f_I \ln\left(\dfrac{1 + b_I P_\delta}{1 + b_I P_0}\right)}\right] \tag{10}$$

$$C1 = \left[\frac{b_C f_C^2}{(1 + b_C P_\delta)(1 + b_C P_0)} + \frac{b_I f_I^2}{(1 + b_I P_\delta)(1 + b_I P_0)} \right] \tag{10a}$$

$$C2 = \left[f_C^2 - 2 f_C f_I \left(\frac{b_I}{b_C - b_I} \right) \right] \tag{10b}$$

$$C3 = \left[f_I^2 + 2 f_C f_I \left(\frac{b_C}{b_C - b_I} \right) \right] \tag{10c}$$

The transient permeate responses, J_{out}, to feed step changes are measured and integrated

$$A \int_0^\infty (J_{SS} - J_{out}) dt = Q_s \tag{11}$$

(J_{SS} = steady state flux) and Q_t is calculated from

$$Q_t = F Q_s \tag{12}$$

where F is a factor relating the integrated fluxes into and out of the membrane

$$F = \frac{\int_0^{t_{SS}} (J_{in} - J_{out}) dt}{\int_0^{t_{SS}} (J_{SS} - J_{out}) dt} = \frac{Q_t}{A \left(J_{SS} t_{SS} - \int_0^{t_{SS}} J_{out} dt \right)} \tag{13}$$

When the coverage at the permeate boundary is zero, the single component F-factor is 3 for Fickian diffusion. For Maxwell–Stefan surface diffusion, the F-factor (Gardner et al., 2003) depends on the feed-side fractional coverage θ_0

$$F_{MS,0} = \frac{2 \ln(1 - \theta_0)[\theta_0 + \ln(1 - \theta_0)]}{2\theta_0 + \ln(1 - \theta_0)[2 + \ln(1 - \theta_0)]} \tag{14}$$

As θ_0 increases from 0 to 1, $F_{MS,0}$ decreases from 3 to 2. Support resistance at the permeate boundary causes the F-factors to increase (Gardner et al., 2003). When the permeate coverage is not zero, the F-factors must be determined iteratively, as described in the section on numerical solution of the transient model.

The sum of squared errors (*SSE*) between the measured Q_t and the modeled ($Q_c - n_i$)

$$SSE = \sum_{allPo's} [Q_t - (Q_c - n_i)]^2 \tag{15}$$

was minimized for a series of feed partial pressures by varying parameters δ, q_{sat}, and b in Q_c for single-site and δ, b_C, and b_I for dual-site Langmuir adsorption. Because Q_t is the incremental number of moles adsorbed between the time of the step change and when the new steady state was attained, and Q_c is the total number of moles adsorbed in the membrane for a given feed partial pressure, the number of moles adsorbed in the membrane at the beginning of the step change (n_i) must be subtracted from Q_c in Eq. 15.

Diffusion

Once the adsorption parameters and effective membrane thickness were determined from the above analysis, the Maxwell–Stefan diffusivities were calculated from the steady state fluxes by

$$\frac{Đ_{MS}}{\delta} = \frac{J_{SS}}{\rho \ln\left(\frac{1 + bP_0}{1 + bP_\delta} \right)^{q_{sat}}} \tag{16}$$

for single-site Langmuir adsorption and

$$\frac{Đ_{MS}}{\delta} = \frac{J_{SS}}{\rho \ln\left[\left(\frac{1 + b_C P_0}{1 + b_C P_\delta} \right)^{q_{satC}} \left(\frac{1 + b_I P_0}{1 + b_I P_\delta} \right)^{q_{satI}} \right]} \tag{17}$$

for dual-site Langmuir adsorption. These equations result from integrating the equation for flux ($J = J_{out}$, applied at $z = \delta$) written in terms of P

$$J_{out} = -\rho Đ_{MS} \Gamma \left. \frac{\partial q}{\partial z} \right|_{z=\delta} = -\rho q_{sat} Đ_{MS} \frac{q}{P} \left. \frac{\partial P}{\partial z} \right|_{z=\delta} \tag{18}$$

from $z = 0$ ($P = P_0$) to $z = \delta$ ($P = P_d$).

Numerical solution of the transient model

When all parameters were estimated, Eq. 3 was solved numerically by the method of lines, and the transient coverage profiles and fluxes into and out of the membrane were obtained. As done previously for butane isomers in H-ZSM-5 membranes (Gardner et al., 2002b), the F-factors were determined iteratively using the transient model by the following steps:

(1) Assume factor (F) for each feed condition is that calculated from Eq. 14 to obtain Q_t values from the measured transients.

(2) Minimize *SSE* for all conditions for one temperature to obtain δ, q_{sat}, and b (for single-site Langmuir isotherm) or δ, b_C, and b_I (for dual-site Langmuir isotherm).

(3) Run transient Maxwell–Stefan numerical model to obtain J_{in}, J_{out}, and coverage profiles.

(4) Numerically integrate elements in Eq. 13 to obtain new F for each feed condition.

(5) Use new F-values to obtain new Q_t values from the measured transients.

(6) Repeat steps 2–5 until adsorption parameters and δ change by less than 1% of their value.

Permeance and selectivity

Permeation measurements in membranes are usually reported in terms of permeance, $\Pi = J/\Delta P_i$ (mol/m^2 s Pa), since the fluxes depend on the partial pressure drop across the membrane (ΔP_i), and selectivities are reported as ratios of per-

meances. This is a convenient way to normalize the fluxes because the pressure drop is usually known. Note that when ΔP is the same for two permeants the permeance selectivity is the ratio of fluxes because the partial pressure drop cancels.

The driving force for diffusion through zeolite membranes, however, is the chemical potential gradient, which is better approximated by the coverage gradient than the pressure drop across the membrane. At 295 K, silicalite-1 is saturated with n-C_4 at a partial pressure of 20 kPa. Thus, increasing the n-C_4 feed partial pressure above 20 kPa (thus increasing the partial pressure drop) would decrease the permeance, even though the flux and driving force remain constant. Similarly, for the same partial pressure drop across a membrane, the driving force for diffusion of two permeants can be different. For example, in a silicalite-1 membrane at 295 K with feed and permeate partial pressures of 120 and 5 kPa, respectively, $\Delta\theta_{\text{n-C4}} = 0.08$ and $\Delta\theta_{\text{i-C4}} = 0.4$ (using adsorption data of Zhu et al., 2000). Therefore, to properly interpret differences in (or ratios of) permeances, the operating conditions and associated coverages should be known. Because the adsorption properties of the transport pathways are measured by the transient permeation method, the real driving force for diffusion through zeolite membranes can be calculated.

The permeance selectivity can be written in terms of the partial pressure drop, Maxwell–Stefan diffusivity, and driving force ratios as

$$\frac{\Pi_1}{\Pi_2} = \frac{\Delta P_2}{\Delta P_1}\frac{Đ_{\text{MS},1}}{Đ_{\text{MS},2}}\frac{\left(\Gamma_\delta \left.\frac{\partial q}{\partial z}\right|_\delta\right)_1}{\left(\Gamma_\delta \left.\frac{\partial q}{\partial z}\right|_\delta\right)_2} \tag{19}$$

Here the coverage gradients, ∇q, are written as partial derivatives in the z-direction because we are considering one-dimensional diffusion. When the partial pressure drops across a membrane are equal for two components, the permeance selectivity is the product of a diffusion ratio and an adsorption ratio. By looking at these ratios separately, the trends in the permeance selectivities can be better understood.

Experimental Methods

Al-ZSM-5 gel preparation

The Al-ZSM-5 membrane was prepared by an alkali-free method (Tuan et al., 1999). Silica sol (Ludox AS-40) was the silicon source, aluminum isopropoxide (Aldrich, 98+%) was the aluminum source, and tetrapropylammonium hydroxide (TPAOH) was the template for ZSM-5 synthesis. A clear gel with a molar composition of 438 H_2O:19.5 SiO_2:0.0162 Al_2O_3:1 TPAOH was used.

In a 250-mL beaker with a magnetic stirring bar, 29 mg aluminum isopropoxide (Aldrich, 98+%) was dissolved in 4 g isopropanol (Fisher, 99.9%). The solution was stirred 5 min. Then 4.5 g TPAOH (Aldrich, 1 M solution) was added and the solution stirred 20–30 min until transparent. In a separate 250-mL beaker, 12.98 g Ludox AS-40 (40% SiO_2) was added to 26.98 g deionized H_2O. When the first solution was clear, the SiO_2 and water were poured slowly into it while stirring. The combined solution was stirred for 1 h, and the clear solution was poured into a plastic bottle, capped, and aged overnight before being used in synthesis.

Table 1. Membrane Synthesis Conditions and Estimated Effective Thicknesses

Membrane	Si/Me Ratio	Synthesis Time per Layer (h)	Synthesis Temperature (K)	Support	δ (μm)
Al-ZSM-5	600	48, 48, 48	458	Stainless steel	220
Al-ZSM-11	600	24, 72, 72	403	α-Alumina	190
B-ZSM-5	100	22, 48, 48	458	Stainless steel	320

B-ZSM-5 gel preparation

The boron-substituted ZSM-5 membrane was also prepared by an alkali-free method (Tuan et al., 2000b). The boron source was boric acid (Aldrich, 99.5%) and the molar composition of the gel was 0.195 $B(OH)_3$:1.55 TPAOH:19.46 SiO_2:438 H_2O. The gel synthesis and ageing procedures were the same as those for the Al-ZSM-5 gel, but 54 mg of boric acid was added in place of the aluminum isopropoxide and 7 g TPAOH was used rather than 4.5 g.

Al-ZSM-11 gel preparation

Tetra-butyl-ammonium hydroxide (TBAOH) was the template in MEL membrane preparation. The gel for the MEL membrane (Tuan et al., 2001) had a molar composition of 1.25 Na_2O:0.0162 Al_2O_3:1.5 TBAOH:19.5 SiO_2:438 H_2O where Ludox AS-40 (silica sol) and sodium aluminate ($Na_2Al_2O_4$) were used as the Si and Al sources, respectively. The Si/Al ratio was 600, as it was for the Al-ZSM-5 gel. The synthesis and ageing procedures were the same as those for the Al-ZSM-5 gel.

Membrane synthesis

The synthesis procedure was the same for all three membranes, although the support material and synthesis temperature and times were different. The conditions are summarized in Table 1. The sintered stainless steel tubes (Mott Metallurgical, i.d. 0.65 cm, o.d. 0.95 cm, 2.7 cm long) had a nominal pore size of 0.5 μm. One-centimeter lengths of solid 304L stainless steel tubing were welded onto the ends of the sintered metal supports to provide a surface for sealing the membranes into the module. The α-alumina support (US Filter, i.d. 0.7 cm, o.d. 1 cm, 4.7 cm long) had a nominal pore size of 0.2 μm. One centimeter at each end was glazed (GL 611A, Duncan) to provide nonporous surfaces for sealing the membrane into the module.

One end of the support tube was wrapped in Teflon tape and covered with a Teflon cap and the support was filled with about 2 mL of synthesis gel. As the gel soaked into the porous support, the tube was refilled throughout the day. The support was allowed to soak overnight and was refilled three more times the following day. The other end was then wrapped with Teflon tape and covered with a Teflon cap and the tube was placed in a Teflon-lined autoclave. The first zeolite layer was synthesized and the tube was then rinsed with D.I. water, brushed gently on the inside surface to remove loose crystals, and dried for 10 min in a vacuum oven at 383 K. After

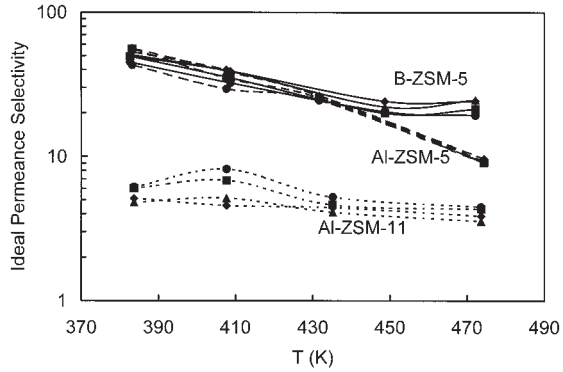

Figure 1. Ideal n-C_4/i-C_4 permeance selectivities in zeolite membranes as a function of temperature for four feed concentrations of butane (● = 5%, ■ = 20%, ▲ = 50%, ◆ = 100%) in helium.

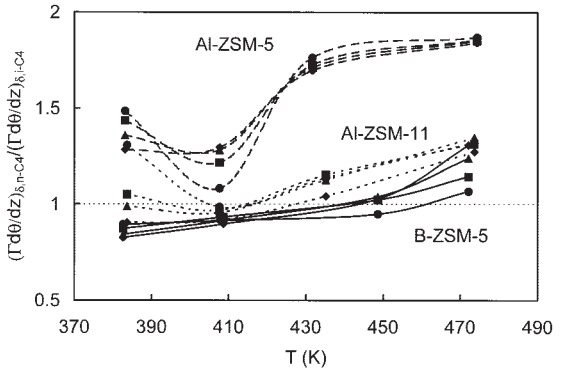

Figure 3. Ratios of the single-component adsorption driving forces for 5 (●), 20 (■), 50 (▲), and 100 (◆) % n-C_4 and i-C_4 in helium through zeolite membranes as a function of temperature.

synthesis of each layer, N_2 at 138 kPa was fed to the membrane to determine whether the zeolite layer was gas tight. If N_2 permeation was detected, another layer was added with the membrane's vertical orientation in the autoclave switched for each subsequent layer. The membranes required three layers before being impermeable to N_2 before calcination. After the third synthesis, the membranes were dried in a vacuum oven at 383 K overnight and calcined in stagnant air at 758 K for 8 h (heated and cooled at 0.01 and 0.018 K/s, respectively).

Because the membranes were synthesized on the inside surfaces of tubular supports, their structures, morphologies, and chemical compositions could not be measured without destroying the membranes. The Si/Al and Si/B ratios reported here are those of the synthesis gel. The zeolite structure and film morphology of similarly made membranes were previously determined by XRD and SEM analysis (Tuan et al., 1999, 2000b, 2001). Chemical analyses of the metal content of similarly made membranes in our laboratory indicated that the Si/(substitution metal) ratio of the membrane was approximately twice that of the parent gel (Li et al., 2003). The chemical composition of similar membranes was also previously measured as a function of thickness (Poshusta et al., 2000).

Transient permeation measurements

A Wicke–Kallenbach system (Bakker et al., 1996), with helium as the carrier gas and feed diluent, was used for the transient permeation measurements. The membranes were sealed in a stainless steel module with Viton O-rings on each end. The module and feed line were wrapped with heating tape controlled by a variac. Before each measurement, helium flowed on the feed (inside of the tube) and permeate sides of the membrane, and the module was heated to 473 K to remove adsorbed species from the membrane. The permeate total pressure was about 82 kPa (atmospheric pressure in Boulder, CO). The feed total pressure was about 120 kPa for the Al-ZSM-5 and B-ZSM-5 membranes. The total feed pressure was about 82 kPa for the Al-ZSM-11 membrane, except when i-C_4 was used at 406 K. Two feed gas streams, each containing helium, butane, or a mixture of the two, flowed at 100 cm^3/min (standard temperature and pressure) to a manual switching valve

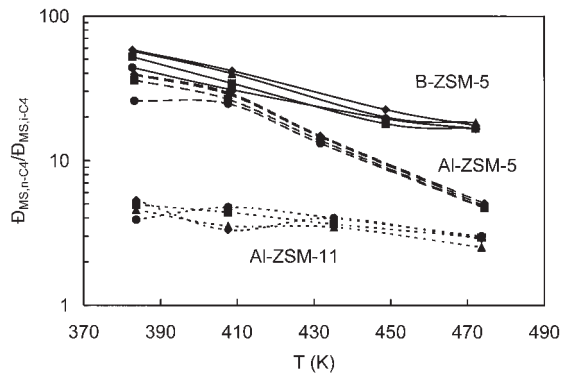

Figure 2. Ratios of the single-gas n-C_4/i-C_4 Maxwell–Stefan diffusivities for 5 (●), 20 (■), 50 (▲), and 100 (◆) % n-C_4 and i-C_4 in helium through zeolite membranes as a function of temperature.

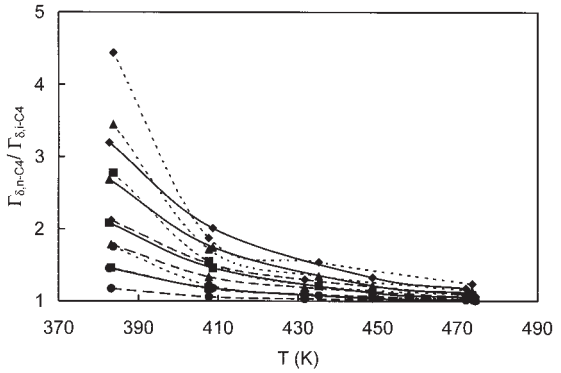

Figure 4. Ratios of the thermodynamic correction factors at the permeate boundary for 5 (●), 20 (■), 50 (▲), and 100 (◆) % n-C_4 and i-C_4 in helium through B-ZSM-5 (solid lines), Al-ZSM-5 (dashed lines), and Al-ZSM-11 (dotted lines) zeolite membranes as a function of temperature.

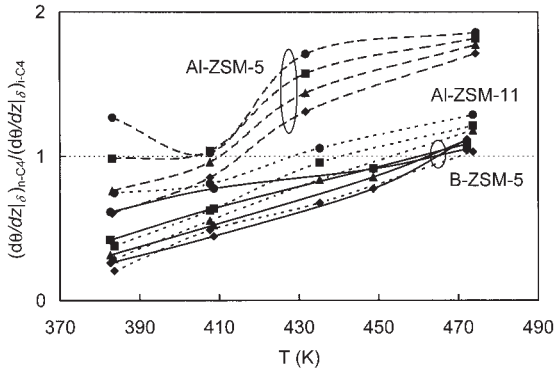

Figure 5. Ratios of the coverage gradients at the permeate boundary for 5 (●), 20 (■), 50 (▲), and 100 (◆) % n-C_4 and i-C_4 in helium through zeolite membranes as a function of temperature.

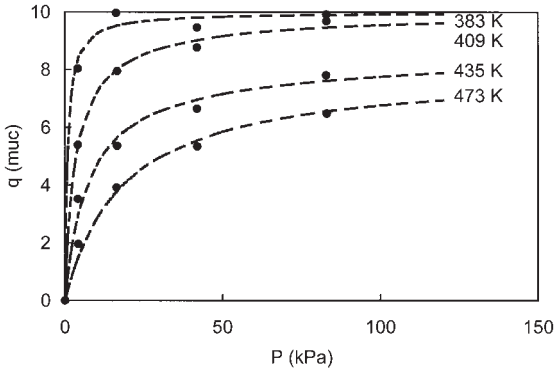

Figure 7. Adsorption isotherms for n-C_4 in an Al-ZSM-11 zeolite membrane.

The points are from transient experiments, and the dashed lines are the dual-site Langmuir adsorption model.

that sent one inlet to a vent and the other to the membrane feed side. Initially helium flowed to the membrane and 5% butane flowed to the vent. The valve was switched so 5% butane fed the membrane, and the other feed line concentration was then changed to 20% butane in helium. When the permeate concentration reached steady state, the valve was switched so that 20% butane flowed to the membrane. The feed concentration was thus increased stepwise to 50 and 100% butane and then decreased from 100 to 5% butane without desorbing butane between changes. Back-pressure regulators on the retentate and bypass lines were adjusted so both feed pressures were at 120 kPa (or 82 kPa) and did not change when the valve was switched. The responses in the permeate concentration to these step changes in the feed were measured with a quadrupole mass spectrometer (Pfeiffer Vacuum Prisma) that monitored multiple mass peaks simultaneously. The total flow rates were measured with a bubble flow meter.

Results

Membrane effective thickness

The effective membrane thicknesses determined from the transient permeation analysis are listed in Table 1. The Al-ZSM-5 membrane was used previously in transient permeation experiments of light gases (Gardner et al., 2002a) and butane isomers (Gardner et al., 2002b). Single-site Langmuir adsorption was used in the model for these gases. The effective thickness determined from both light gases and butane was 220 μm, as it was in the current study. Another Al-ZSM-5 membrane analyzed simultaneously by the light gas transient permeation responses had an effective thickness of 250 μm. These effective thicknesses were approximately twice the thickness estimated from SEM images of a film synthesized with one layer instead of three. The higher effective thickness was attributed to the extra synthesis layers and to transport through crystals in the support layer. The effective thicknesses of the Al-ZSM-11 and B-ZSM-5 membranes are within 30% of those determined previously for Al-ZSM-5 membranes.

Ideal selectivities

The n-C_4/i-C_4 ideal permeance selectivities of the three membranes at steady state are shown in Figure 1 for four butane feed concentrations. The ideal selectivities based on permeance are essentially the flux selectivities, given that the partial pressure drops were approximately the same for n-C_4 and i-C_4 for each point. The ideal selectivity tends to decrease with increasing temperature, but does not correlate with butane

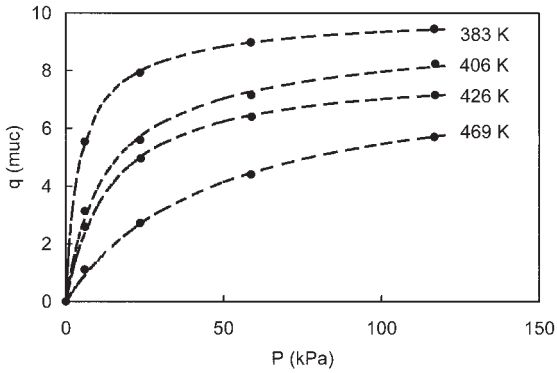

Figure 6. Adsorption isotherms for n-C_4 in an Al-ZSM-5 zeolite membrane.

The points are from transient experiments, and the dashed lines are the dual-site Langmuir adsorption model.

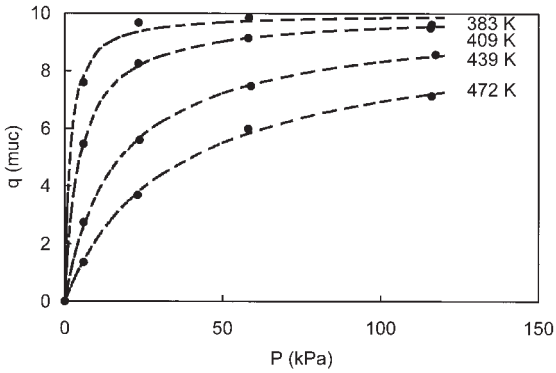

Figure 8. Adsorption isotherms for n-C_4 in a B-ZSM-5 zeolite membrane.

The points are from transient experiments, and the dashed lines are the dual-site Langmuir adsorption model.

Table 2. Dual-Site Langmuir Adsorption Isotherm Parameters Obtained from Transient Permeation Analysis of Zeolite Membranes*

	n-C_4			i-C_4		
Membrane	T (K)	b_C (kPa^{-1})	b_I (kPa^{-1})	T (K)	b_I (kPa^{-1})	b_C (kPa^{-1})
Al-ZSM-5	383	0.30	0.041	383	0.34	0.0090
	406	0.092	0.0060	409	0.17	0.0024
	426	0.071	—	437	0.076	—
	469	0.022	—	480	0.022	—
Al-ZSM-11	383	1.2	1.2	384	1.2	0.086
	409	0.38	0.071	406	0.43	0.034
	435	0.14	0.0017	435	0.19	0.013
	473	0.054	—	474	0.066	0.0042
B-ZSM-5	382	0.63	0.63	383	2.0	0.097
	408	0.27	0.075	409	0.56	0.050
	449	0.074	0.018	448	0.14	0.014
	470	0.034	0.0059	474	0.063	—

*Site C represents the channels in the MFI and MEL zeolite structures with $q_{satC,n\text{-}C4} = 8$ and $q_{satC,i\text{-}C4} = 6$ molec./u.c.; site I represents intersections with $q_{satI,n\text{-}C4} = 2$ and $q_{satI,i\text{-}C4} = 4$ molec./u.c.

feed concentration. The selectivity was separated into the ratios of the Maxwell–Stefan diffusivities, calculated as outlined in the section on modeling, in Figure 2, and the ratios of the adsorption driving forces in Figure 3. The adsorption driving forces are further separated into the ratios of the thermodynamic correction factors (Figure 4) and the coverage gradients (Figure 5) at the permeate boundary.

The ratio of the Maxwell–Stefan diffusivities decreases with temperature and tends to increase with increasing feed concentration for all three membranes. The diffusivity ratio increases in the order Al-ZSM-11 < Al-ZSM-5 < B-ZSM-5 for the conditions studied and depends less on feed concentration at higher temperatures. The ratio of the thermodynamic correction factors (Figure 4) is higher at high coverages, that is, at low temperatures and high feed concentrations. As the temperature increases, the thermodynamic correction factors for each isomer approach 1. The coverage gradient ratios, on the other hand, tend to increase with increasing temperature and decrease with increasing feed concentration (Figure 5). Because of the competing effects of these two adsorption terms, the ratios of adsorption driving forces can go through minima with

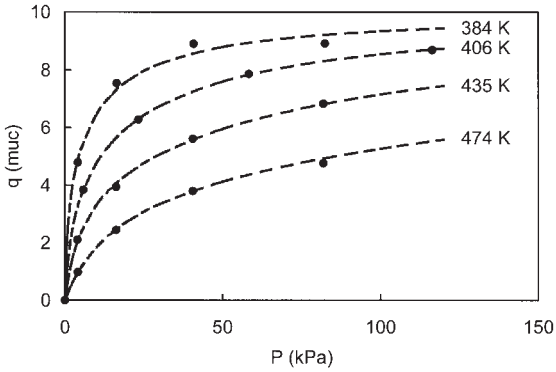

Figure 10. Adsorption isotherms for i-C_4 in an Al-ZSM-11 zeolite membrane.

The points are from transient experiments, and the dashed lines are the dual-site Langmuir adsorption model.

temperature, as shown in Figure 3, for the lower coverages in the Al-substituted membranes. The n-C_4 driving forces are all higher than those for i-C_4 in the Al-ZSM-5 membrane, but i-C_4 has a higher driving force than n-C_4 at the lower temperatures and higher feed partial pressures in the B-ZSM-5 and Al-ZSM-11 membranes.

Adsorption isotherms

The n-C_4 dual-site adsorption isotherms measured in the membranes are shown in Figures 6–8. The adsorption equilibrium constants for each site ($q_{satC} = 8$ molec./u.c. and $q_{satI} = 2$ molec./u.c.) obtained for each isotherm are listed in Table 2. The adsorption equilibrium constants increase in the order Al-ZSM-5 < B-ZSM-5 < Al-ZSM-11; these values indicate that the MEL membrane pores fill with n-C_4 at lower pressures than do those of the MFI membranes. For isotherms where the n-C_4 coverage was less than 8 molec./u.c. at 120 kPa, the intersection adsorption equilibrium constants could not be estimated by the transient method.

The i-C_4 dual-site adsorption isotherms are shown in Figures 9–11, and the adsorption equilibrium constants for each site ($q_{satI} = 4$ molec./u.c. and $q_{satC} = 6$ molec./u.c.) are given in Table 2. The i-C_4 coverages in the Al-ZSM-5 membrane are

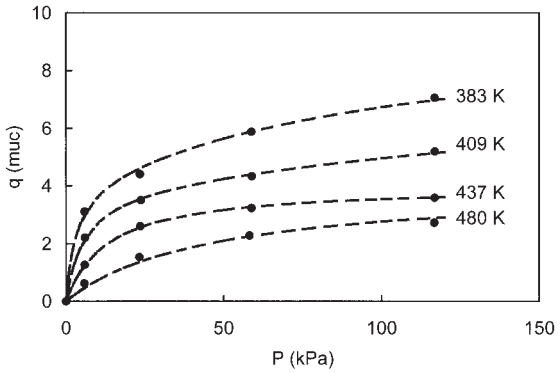

Figure 9. Adsorption isotherms for i-C_4 in an Al-ZSM-5 zeolite membrane.

The points are from transient experiments, and the dashed lines are the dual-site Langmuir adsorption model.

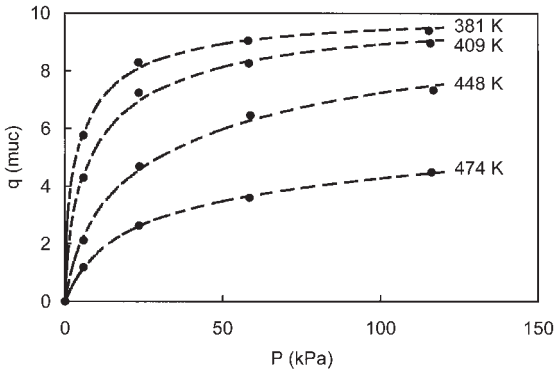

Figure 11. Adsorption isotherms for i-C_4 in a B-ZSM-5 zeolite membrane.

The points are from transient experiments, and the dashed lines are the dual-site Langmuir adsorption model.

Table 3. Single-Site Langmuir Adsorption Isotherm Parameters in Al-ZSM-5, Al-ZSM-11, and B-ZSM-5 Membranes Obtained from Transient Permeation Analysis and in Silicalite Powder Measured by TEOM (Zhu et al., 1998)

	n-C_4			i-C_4		
	T (K)	q_{sat} (molec./u.c.)	b (kPa^{-1})	T (K)	q_{sat} (molec./u.c.)	b (kPa^{-1})
Al-ZSM-5	383	9.0	0.27	383	4.0	0.45
membrane;	406	8.3	0.091	409	3.8	0.23
transient	426	8.1	0.073	437	3.8	0.090
permeation	469	7.8	0.024	480	3.0	0.039
Al-ZSM-11	383	9.8	0.75			
membrane;	409	9.3	0.31			
transient	435	7.8	0.15			
permeation	473	7.2	0.072			
B-ZSM-5	382	9.9	0.67			
membrane;	408	9.7	0.23			
transient	449	9.3	0.066			
permeation	470	8.9	0.032			
	373	6.9	0.24	373	3.4	0.30
Silicalite powder;	408	6.6	0.064	408	3.3	0.093
TEOM (Zhu et	438	6.1	0.024	438	3.2	0.039
al., 1998)	473	5.0	0.013	473	3.2	0.016

lower than those in the other two membranes at a given temperature and pressure, as was true for n-C_4 coverages. At 437 and 480 K, the i-C_4 coverage in the Al-ZSM-5 membrane was below 4 molec./u.c. at 120 kPa, so the second site adsorption equilibrium constants could not be estimated at these temperatures. In the other two membranes, the second site contributes to the total saturation coverage at 120 kPa even at 474 K. At 381–384 K, the Al-ZSM-11 and B-ZSM-5 membranes were almost saturated at 10 molec./u.c., whereas the coverage in the Al-ZSM-5 membrane was only approximately 7 molec./u.c.

Single-site vs. dual-site fitting

The n-C_4 isotherms in the three membranes and the i-C_4 isotherms in the Al-ZSM-5 membrane were also fit with a single-site model that estimated q_{sat} and b. Because the coverage is not measured directly by the transient method, the points on the adsorption isotherms were determined by the iterative fitting procedure and were therefore different when the transients were fit with the dual- and single-site models. Thus, the q_{sat} values for the single-site model were not forced to be near 8 or 10 molec./u.c. for n-C_4 or 4 or 10 molec./u.c. for i-C_4. The q_{sat} and b values are comparable to single-site parameters measured under similar conditions by the tapered element oscillating microbalance (TEOM) technique for silicalite powder (see Table 3). The estimated q_{sat} values were between 7 and 10 molec./u.c. for n-C_4 and were approximately 4 molec./u.c. for i-C_4 except at the highest temperature where q_{sat} was about 3 molec./u.c. The estimated q_{sat} values decreased with increasing temperature, as was previously found (Gardner et al., 2002a,b; Zhu et al., 1998). The b values for the single-site n-C_4 model fits were approximately the same as the dual-site b_C values in all cases. The i-C_4 single-site model b values in the Al-ZSM-5 membrane were slightly higher than the dual-site b_I values.

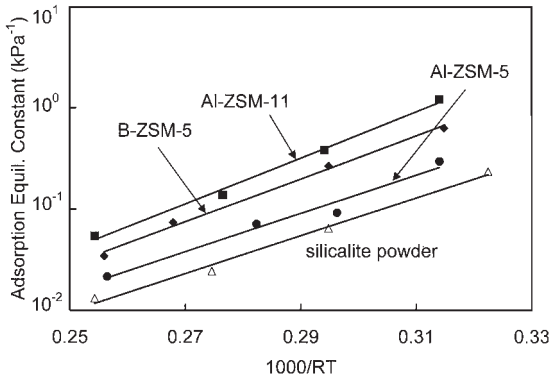

Figure 12. Adsorption equilibrium constants vs. inverse temperature for n-C_4 adsorption in the channels of zeolite membranes.

A dual-site Langmuir model was used to model the transient permeation data. Equilibrium constants for silicalite crystals were measured by TEOM in Zhu et al. (1998), assuming single-site Langmuir adsorption.

Thermodynamic properties

The heats and entropies of adsorption from the Arrhenius plots of the adsorption equilibrium constants (Figures 12–14) are listed in Table 4 (error estimates are standard deviations). The n-C_4 adsorption equilibrium constants in the intersection sites were not estimated accurately enough to justify an Arrhenius plot because the n-C_4 coverages were below 8 molec./u.c. for some conditions and only slightly above 8 molec./u.c. for others. The adsorption equilibrium constants estimated for i-C_4 in the channels are also likely to have more error than those measured for the "first" adsorption sites. The first adsorption site is defined by convention as the one with the higher adsorption equilibrium constant. However, given that the highest i-C_4 coverages were significantly above 4 molec./u.c. in most cases, the b_C estimates for i-C_4 were better than the b_I estimates for n-C_4, and the thermodynamic properties are therefore reported.

All the adsorption equilibrium constants have the expected

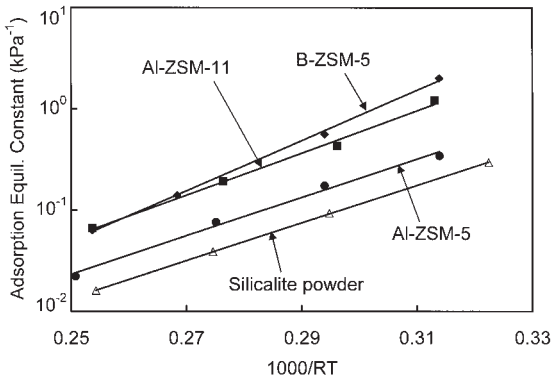

Figure 13. Adsorption equilibrium constants vs. inverse temperature of i-C_4 in the intersections of zeolite membranes.

A dual-site Langmuir model was used to model the transient permeation data. Equilibrium constants for silicalite crystals were measured by TEOM in Zhu et al. (1998), assuming single-site Langmuir adsorption.

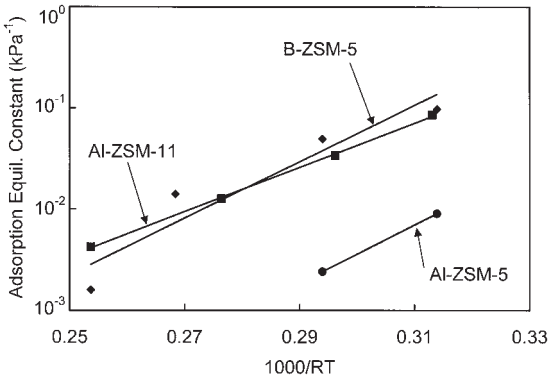

Figure 14. Dual-site Langmuir adsorption equilibrium constants vs. inverse temperature of i-C_4 in the channels of zeolite membranes measured by the transient permeation method.

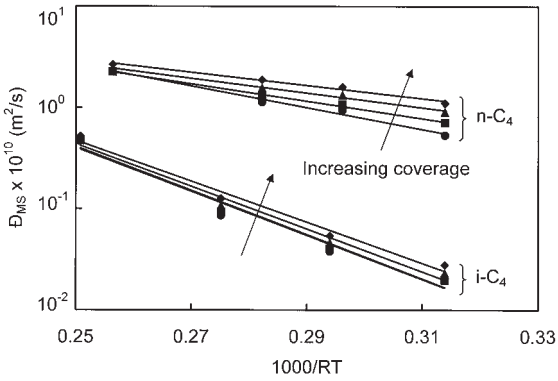

Figure 15. Maxwell–Stefan diffusivities vs. inverse temperature for n-C_4 and i-C_4 diffusion through the Al-ZSM-5 membrane (●) 5%, (■) 20%, (▲) 50%, and (◆) 100% butane in helium.

exponential dependency on temperature, and the heats and entropies of adsorption are in the ranges reported in the literature for MFI-type powders. In Figures 12 and 13, the single-site adsorption equilibrium constants measured by TEOM on silicalite-1 powder are shown for comparison. The q_{sat} values obtained from the single-site fit of i-C_4 adsorption on the silicalite powder were just below 4 molec./u.c., so the second site had not yet begun to contribute significantly to the adsorption. Thus the i-C_4 adsorption equilibrium constants for silicalite-1 are compared to those measured for the intersections by the dual-site model. Of the three membranes, the n-C_4 and i-C_4 adsorption equilibrium constants for Al-ZSM-5 are the closest to those measured for the silicalite powder. A smaller change in entropy upon adsorption (smaller $|-\Delta S_{ads}|$) shifts b higher on an Arrhenius plot and a higher heat of adsorption (larger $|-\Delta H_{ads}|$) increases the slope. The n-C_4 adsorption equilibrium constants are highest in the Al-ZSM-11 membrane, indicating that the entropy changes less upon adsorption of n-C_4 in the Al-ZSM-11 than in the ZSM-5 membranes. The heats of adsorption of n-C_4 are approximately the same in the three membranes. The heat of adsorption of i-C_4 in the intersections of the B-ZSM-5 membrane is slightly higher than those in the Al-substituted membranes.

Diffusivities

The Maxwell–Stefan diffusivities measured in the membranes are shown in Figures 15–17. The exponents of the preexponentials and the activation energies for diffusion for each feed concentration are given in Table 5 (error estimates are standard deviations). The activation energies are similar to those reported for polycrystalline silicalite membranes, single crystal membranes, and by PFG-NMR and frequency response measurements for crystals (Gardner et al., 2002b). The Maxwell–Stefan diffusivities increase with increasing feed partial pressure at a given temperature, as previously found for light gases and butane isomers in ZSM-5 membranes (Gardner et al., 2002a,b). The diffusivities generally vary less with feed partial pressure at higher temperatures, where the coverages are lower, and the i-C_4 diffusivities in the B-ZSM-5 membrane vary least with coverage. The spread in the diffusivities with feed partial pressure in the Al-ZSM-11 membrane is higher for the i-C_4 measurements made at 406 K (1000/RT = 0.296) than at the other temperatures. At this temperature the total feed pressure for the i-C_4 measurements was approximately 120 kPa and at the other temperatures (and at all temperatures for n-C_4) it was about 82 kPa.

The preexponentials for diffusion decrease [$\ln(Đ_{MS,0})$ be-

Table 4. Heats and Entropies of Adsorption from Transient Permeation Analysis on Membranes and from the Literature for Silicalite Powders

	n-C_4		*i-C_4*			
Membrane	$-\Delta H_{adsC}$ (kJ/mol)	$-\Delta S_{adsC}$ (J/mol K)	$-\Delta H_{adsI}$ (kJ/mol)	$-\Delta S_{adsI}$ (J/mol K)	$-\Delta H_{adsC}$ (kJ/mol)	$-\Delta S_{adsC}$ (J/mol K)
Al-ZSM-5	44 ± 5	130 ± 12	44 ± 3	120 ± 6	66*	210*
Al-ZSM-11	52 ± 3	140 ± 7	48 ± 3	120 ± 6	50 ± 1	150 ± 2
B-ZSM-5	49 ± 2, 75 ± 8 (I)	130 ± 6, 200 ± 18 (I)	57 ± 2	140 ± 4	64 ± 15	180 ± 35
Silicalite-1 powder; TEOM; dual-site combined fitting (Zhu et al., 2000)	56, 50 (I)	113, 126 (I)	46	83	66	202
Silicalite-1 (Millot et al., 1999)			50	88	45	144
Silicalite-1 (MFI); simulation (Schenk et al., 2002)	54, 49 (I)	155, 177 (I)	49	134	43	188
Silicalite-2 (MEL); simulation (Schenk et al., 2002)	51, 52 (I)	154, 189 (I)	49	138	36	175

*Error estimates could not be determined from fit with only two points.

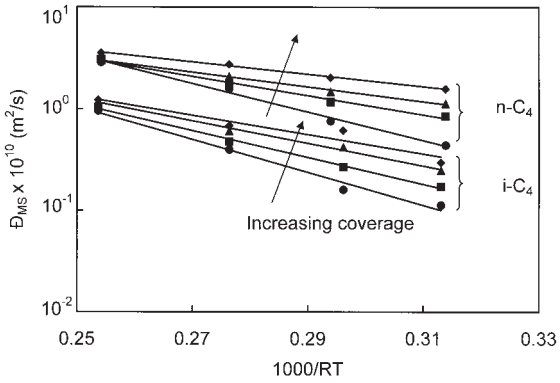

Figure 16. Maxwell–Stefan diffusivities vs. inverse temperature for n-C_4 and i-C_4 diffusion through the Al-ZSM-11 membrane (●) 5%, (■) 20%, (▲) 50%, and (◆) 100% butane in helium.

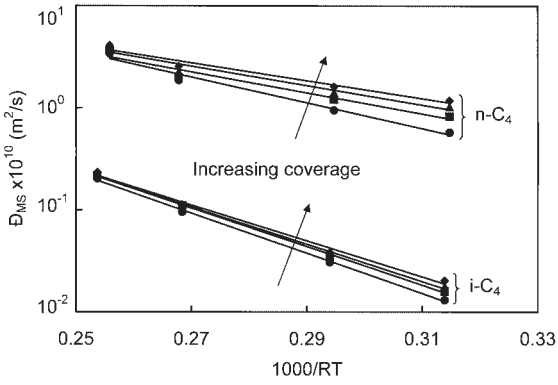

Figure 17. Maxwell–Stefan diffusivities vs. inverse temperature for n-C_4 and i-C_4 diffusion through the B-ZSM-5 membrane (●) 5%, (■) 20%, (▲) 50%, and (◆) 100% butane in helium.

comes more negative] and the activation energies decrease with increasing feed concentration. The most notable differences in Figures 15–17 are that the i-C_4 diffusivities in the Al-ZSM-11 membrane are approximately an order of magnitude higher than those in the ZSM-5 membranes, and the activation energies for i-C_4 diffusion are lower in the Al-ZSM-11 membrane. The n-C_4 diffusivities and activation energies are similar in the three membranes.

Transient permeation

Some representative transient responses and the corresponding modeled responses are given in Figures 18–20. Isobutane in the ZSM-5 membranes takes about 10 times as long as n-C_4 to reach steady state so the plots were chosen to represent the range of times to steady state. The times to reach steady state ranged from less than 1 min (n-C_4 in Al-ZSM-11 at 473 K; Figure 19) to more than 5 h (i-C_4 in B-ZSM-5 at 383 K; Figure 20) and the fluxes varied over two orders of magnitude. These model plots were not obtained by adjusting the parameters to fit the transient data, but by using the adsorption parameters obtained from the integrated transients and the diffusivities calculated from the steady-state fluxes. As we previously found for n-C_4 and i-C_4 in an Al-ZSM-5 membrane (Gardner et al., 2002b), the model fit the data better at the lower coverages and often underpredicted the slope of the rise to steady state. The model fit the n-C_4 transient permeate responses in the B-ZSM-5 membrane almost perfectly for both step increases and decreases at all temperatures, and the i-C_4 transient fits were better in the B-ZSM-5 membrane than in the others.

The i-C_4 transient responses through the B-ZSM-5 and Al-ZSM-5 membranes (Figures 18 and 20) decreased through a minimum when the feed concentration was increased and increased through a maximum when the feed concentration was decreased, as reported previously for i-C_4 in Al-ZSM-5 membranes (Gardner et al., 2002b). Some initial transients, normalized based on the steady-state fluxes preceding each feed concentration change, through the B-ZSM-5 and Al-ZSM-11 membranes are shown in Figures 21–23. The minima and maxima were larger fractions of the preceding steady-state fluxes at higher temperatures (Figure 21) and for bigger i-C_4 feed concentration changes (Figure 22). Figures 21 and 22 show the initial transients for feed step changes to the B-ZSM-5 membrane, but those measured in the Al-ZSM-5 membrane followed the same trends with temperature and concentration. The i-C_4 fluxes through the Al-ZSM-11 membrane exhibited extrema at 406 K but not at the other temperatures (Figure 23). The total feed pressure for the 406 K experiment was about 120 kPa, as it was for all of the ZSM-5 measurements, whereas the total feed pressure for the other Al-ZSM-11 experiments was about 84 kPa (the same as the total permeate

Table 5. Diffusivity Preexponentials and Activation Energies

Membrane	C_4 Feed %	n-C_4 $-\ln(Đ_{MS,0})$*	n-C_4 Ea (kJ/mol)	i-C_4 $-\ln(Đ_{MS,0})$*	i-C_4 Ea (kJ/mol)	Ea_{iC4}/Ea_{nC4}
Al-ZSM-5	5	16 ± 0.6	25 ± 2	11 ± 2	50 ± 7	2.0
	20	17 ± 0.3	20 ± 1	11 ± 2	50 ± 5	2.6
	50	18 ± 0.3	17 ± 1	12 ± 1	48 ± 5	2.9
	100	18 ± 0.4	15 ± 1	12 ± 1	46 ± 4	3.1
Al-ZSM-11	5	14 ± 0.6	32 ± 2	14 ± 0.9	37 ± 3	1.2
	20	16 ± 0.5	22 ± 2	15 ± 0.4	30 ± 1	1.4
	50	18 ± 0.2	17 ± 0.7	16 ± 0.5	26 ± 2	1.5
	100	18 ± 0.2	14 ± 0.7	17 ± 1	22 ± 4	1.6
B-ZSM-5	5	14 ± 0.8	29 ± 3	13 ± 0.3	45 ± 1	1.6
	20	16 ± 1	24 ± 4	14 ± 0.2	44 ± 1	1.8
	50	16 ± 1	22 ± 4	14 ± 0.5	42 ± 2	1.9
	100	17 ± 0.8	20 ± 3	14 ± 0.7	41 ± 2	2.0

*$Đ_{MS,0}$ in m^2/s.

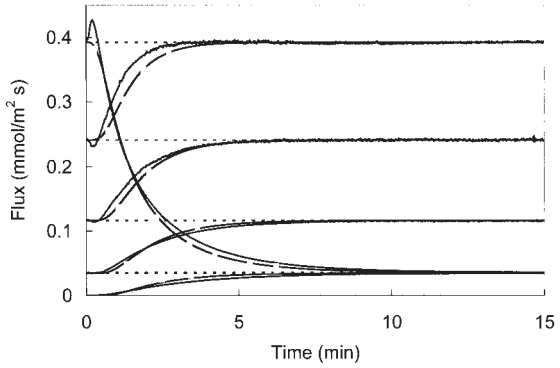

Figure 18. Measured (solid lines) and modeled (dashed lines) i-C_4 permeate responses through an Al-ZSM-5 membrane at 480 K for step changes in the feed.

The feed partial pressure was sequentially increased to 6, 23, 58, and 117 kPa, and then back to 6 kPa. The transients have been shifted on the time axis so that $t = 0$ represents the time of the feed step change for each step.

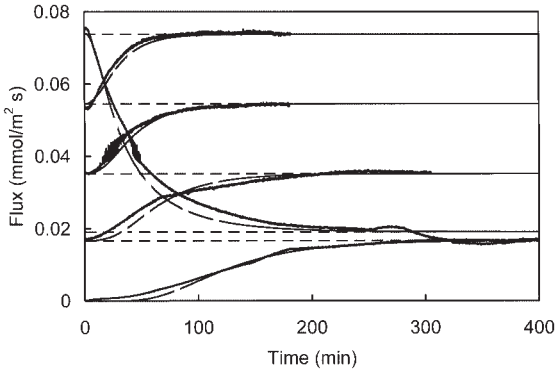

Figure 20. Measured (solid lines) and modeled (dashed lines) i-C_4 permeate responses through a B-ZSM-5 membrane at 383 K for step changes in the feed.

The feed partial pressure was sequentially increased from 0 to 6 kPa, then to 23, 58, and 116 kPa, and then down to 7 kPa. The transients have been shifted on the time axis so that $t = 0$ represents the time of the feed step change for each step.

pressure in all experiments). The n-C_4 transient flux responses did not exhibit measurable minima or maxima with time in any of the membranes under any conditions.

Discussion

Selectivities

The ratios of the n-C_4 to i-C_4 diffusivities (Figure 2) and thermodynamic correction factors (Figure 4) decreased with increasing temperature and decreasing butane concentration in the feed (that is, the ratios were lower for lower coverages). Conversely, the ratio of the coverage gradients (Figure 5) increased with increasing temperature and decreasing butane concentration in the feed. The ratios of the adsorption driving forces were between 0.8 and 1.9. The ratios of the diffusivities were between 5 and 60 for the ZSM-5 membranes and between 2.5 and 5.3 for the Al-ZSM-11 membrane. Therefore, the differences in the diffusion rates of n-C_4 and i-C_4 dominated the selectivities through these membranes under the conditions studied, although in general any or all of the three competitive effects could determine the selectivity.

The diffusivity ratios decreased with increasing temperature (Figure 2) because $Ea_{\text{i-C4}} > Ea_{\text{n-C4}}$. The bulkier i-$C_4$ molecules are more constrained in the zeolite channels than the linear n-C_4 molecules, so the energy barrier that i-C_4 must jump to diffuse from one site to another is higher. Because zeolite pores are close to the size of the butane isomers, small differences in the pore size can significantly affect the activation energies. For example, the activation energy for i-C_4 diffusion is lower in the ZSM-11 membrane than in the ZSM-5 membranes, and thus the i-C_4 diffusivities in the ZSM-11 membrane are almost an order of magnitude higher than those in the ZSM-5 membranes. The lower activation energy and higher diffusivity are

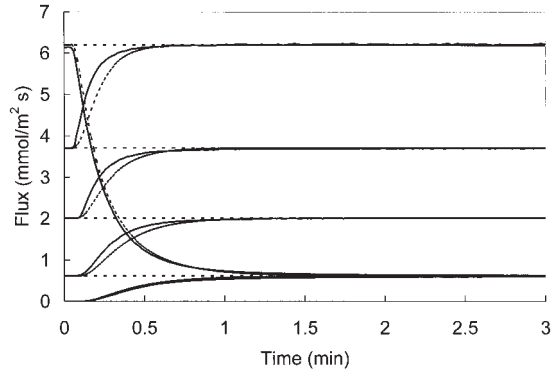

Figure 19. Measured (solid lines) and modeled (dashed lines) n-C_4 permeate responses through an Al-ZSM-11 membrane at 473 K for step changes in the feed.

The feed partial pressure was sequentially increased to 4, 16, 42, and 83 kPa, and then back to 4 kPa. The transients have been shifted on the time axis so that $t = 0$ represents the time of the feed step change for each step.

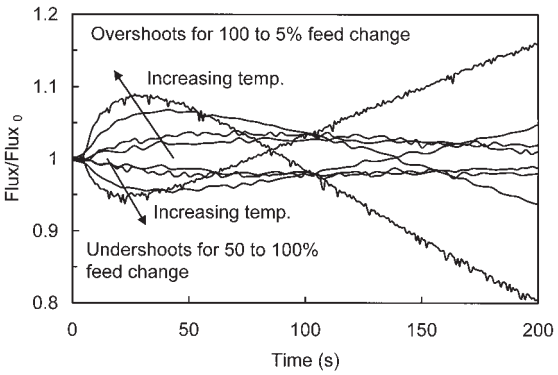

Figure 21. Initial i-C_4 permeate responses through a B-ZSM-5 membrane at 383, 409, 448, and 474 K for step changes in the feed.

For each response the permeate total pressure was 84 kPa, the feed total pressure was about 120 kPa, and the i-C_4 feed concentration (in helium) was increased from 50 to 100% or decreased from 100 to 5%. Each response has been normalized based on the preceding steady state flux.

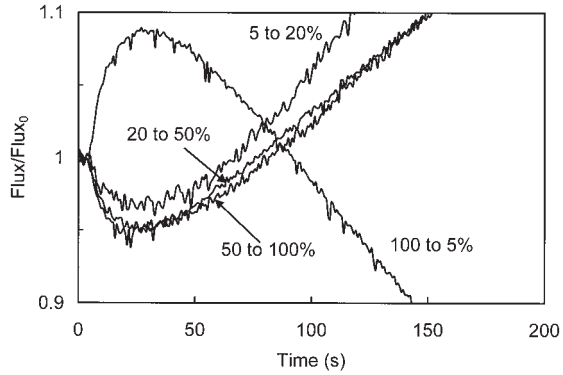

Figure 22. Initial i-C_4 permeate responses through a B-ZSM-5 membrane at 474 K for step changes in the feed.

For each response the permeate total pressure was 84 kPa, the feed total pressure was about 120 kPa, and the i-C_4 feed concentration (in helium) was changed as indicated in the figure. Each response has been normalized based on the preceding steady-state flux.

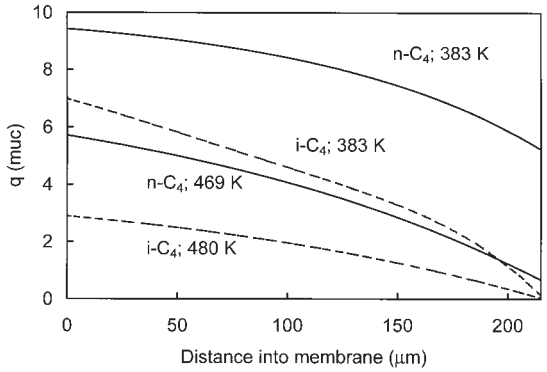

Figure 24. Modeled steady state coverage profiles of n-C_4 (solid lines) and i-C_4 (dashed lines) in an Al-ZSM-5 membrane at 383 and about 475 K.

Feed was 100% butane at about 117 kPa in each case.

most likely because the slightly larger intersections (Maesen et al., 2001), more rounded (5.3 × 5.4 nm compared to 5.1 × 5.7 nm) pores (Meier and Olson, 1992), and straight pathways in MEL constrain i-C_4 significantly less than the elliptical, sinusoidal pores in MFI. Because i-C_4 is bulkier and closer to the size of the pores than n-C_4, these small changes in the framework structure significantly affect i-C_4 diffusion without affecting the more mobile n-C_4 molecules. This explains why the ideal selectivities in the Al-ZSM-11 membrane are an order of magnitude lower than those in the ZSM-5 membranes.

The ratio of the adsorption driving forces is the product of the ratios of the coverage gradients, $(d\theta/dz)_{\delta,\text{n-C4}}/(d\theta/dz)_{\delta,\text{i-C4}}$, and the thermodynamic correction factors, $\Gamma_{\delta,\text{n-C4}}/\Gamma_{\delta,\text{i-C4}}$. The thermodynamic factors correct for the coverage dependency of the transport diffusivity [$J = D_{transport}(dC/dz)$] because the driving force for surface diffusion through zeolites is the chemical potential gradient rather than the gas phase concentration gradient. Krishna et al. (1999) showed that the dual-site thermodynamic correction factors increase with coverage to a maximum at the saturation loading of the first site and then decrease to a minimum between the saturation loadings of the first and second sites. As coverage increases above the point of the minimum, Γ increases again and approaches infinity as θ approaches 1. Under all conditions studied here, the butane coverages for the first site were not saturated at the permeate boundary, so Γ_δ for each isomer increased with increasing coverage.

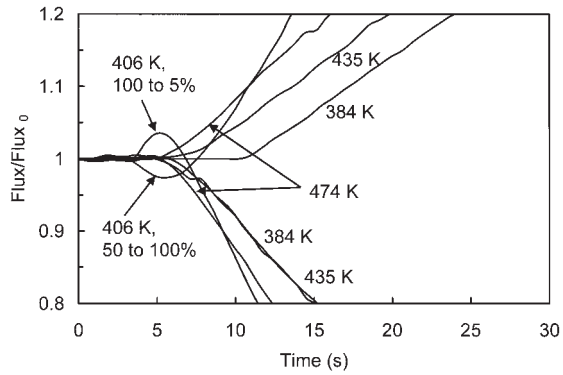

Figure 23. Initial i-C_4 permeate responses through an Al-ZSM-11 membrane at 384, 406, 435, and 474 K for step changes in the feed.

For each response the permeate total pressure was 84 kPa. At 384, 435, and 474 K, the feed total pressure was about 84 kPa and at 406 K the feed total pressure was about 120 kPa. Each response has been normalized based on the preceding steady-state flux.

Because the support essentially acts like a boundary layer of stagnant helium through which the permeating butane must diffuse, low partial pressures of butane at the permeate boundary (from the flux of butane through the membrane) result in nonzero butane coverages on the zeolite at the support interface. The coverages depend on the adsorption equilibrium constants and the partial pressure in the permeate stream. For example, in the Al-ZSM-5 membrane at 373 K the n-C_4 and i-C_4 adsorption equilibrium constants were approximately the same, and the partial pressure of i-C_4 in the permeate was an order of magnitude lower than that of n-C_4 because i-C_4 diffused more slowly. The i-C_4 coverage at the permeate boundary was thus significantly lower than that of n-C_4 (Figure 24; Figure 25 shows the same for the B-ZSM-5 membrane). Consequently, $\Gamma_{\delta,\text{n-C4}}/\Gamma_{\delta,\text{i-C4}}$ was >1 and decreased to 1 with increasing temperature (decreasing coverage) as the Γ values of both isomers decreased to 1. In a similar way, the support resistance caused the coverage gradient in the zeolite at the permeate boundary to be lower for n-C_4 than for i-C_4 when coverages were high. The difference in n-C_4 and i-C_4 permeate boundary coverages is greatest at low temperatures where the diffusion flux difference is greatest and the adsorption equilibrium constants are high. At high temperatures, the fluxes of the isomers were more similar and the adsorption equilibrium constants are lower, so the effect of the support resistance was less important. Thus, as temperature increased the i-C_4 coverage gradients decreased and the n-C_4 coverage gradients did not change much, so $(d\theta/dz\,|_d)_{\text{n-C4}}/(d\theta/dz\,|_d)_{\text{i-C4}}$ increased (Figures 24 and 25).

At high temperatures, the ideal selectivities in the B-ZSM-5 membrane decreased less with increasing temperature than those in the Al-ZSM-5 membrane. Even more interestingly, for

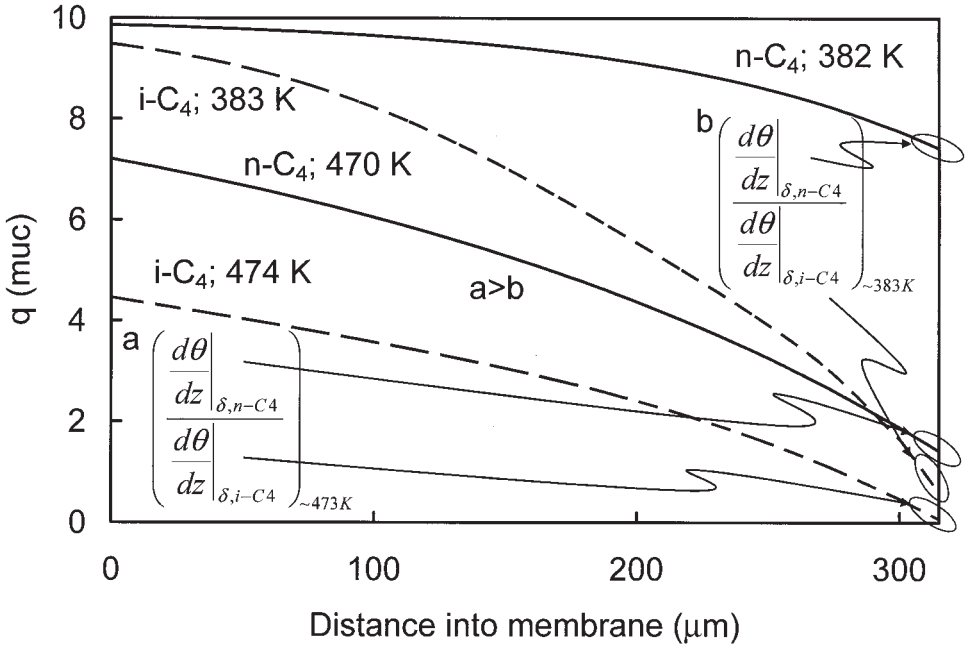

Figure 25. Modeled steady state coverage profiles of n-C_4 (solid lines) and i-C_4 (dashed lines) in a B-ZSM-5 membrane at about 383 and 472 K.

Feed was 100% butane at about 117 kPa in each case.

5 and 20% butane in the feed the B-ZSM-5 ideal selectivities *increased* slightly with temperature. This is because at high temperatures the ratio of the driving forces in B-ZSM-5 (Figure 3) increased more than the diffusivity ratio decreased (Figure 2). The steady-state coverage profiles for 100% butane feed in the B-ZSM-5 membrane at about 383 and 472 K are shown in Figure 25. At 470 K, the fractional coverage of n-C_4 at the permeate boundary is 0.2, so the ratio of driving forces would continue to increase with temperature, and selectivities might be higher above 470 K. This shows that the support can significantly influence selectivity and fluxes in composite zeolite membranes and emphasizes the importance of modeling the support resistance. This also demonstrates that at high temperatures adsorption differences can have a larger influence on the ideal selectivity than diffusion differences in some cases, even though coverages are lower at high temperatures.

The adsorption differences between the two isomers also affected the ideal selectivities through the Al-ZSM-11 membrane. As with the B-ZSM-5 membrane, the ideal selectivities decreased less with temperature between 438 and 473 K than would be predicted by the change in the diffusivities because the ratio of the driving forces increased. Because i-C_4 diffuses much faster through the less constrained MEL pores than it does through the MFI pores, the diffusivities of n-C_4 and i-C_4 in the Al-ZSM-11 membrane were similar. Thus the ideal selectivities were relatively low, and the adsorption differences contributed relatively more to the overall selectivity than in the other two membrane types.

Adsorption isotherms

Molecular simulations showed that the saturation loadings of n-C_4 and i-C_4 in the all-silica forms of MFI (Vlugt et al., 1999) and MEL (Schenk et al., 2002) zeolites are 10 molec./u.c. In MFI and MEL, 4 molec./u.c. of i-C_4 first fill the intersections and at higher pressures 6 more molec./u.c. pack in the channels. In MFI, 8 molec./u.c. of n-C_4 first pack in the channels and at higher pressures 2 more molec./u.c. pack in the intersections (Vlugt et al., 1999). The distinction between the channel and intersection sites was less clear in MEL simulations, and a single-site model fit the simulated data reasonably well. However, when simulated adsorption isotherms in the all-silica forms of ZSM-5 and ZSM-11 zeolites (Schenk et al., 2002) were fit with a single-site model, the estimated q_{sat} values decreased with increasing temperature as they did for the transient measurements in membranes (Table 3). The saturation coverage does not actually decrease with temperature, but q_{sat} tends to be underestimated when the highest pressure (measured or simulated) is below the saturation pressure. Because high pressures are required to saturate the zeolite at high temperatures, the higher-temperature q_{sat} values were underestimated. The adsorption equilibrium constants are more accurately estimated than the q_{sat} values using the single-site model even when the pressures are not high enough to saturate the zeolite because they are related to the slope of the isotherm, which is determined from the lower pressure points. However, to properly estimate and compare heats and entropies of adsorption, the model used to derive the adsorption equilibrium constants must assume a constant saturation coverage. Therefore, the dual-site model with set q_{sat} values and variable adsorption equilibrium constants is more appropriate for modeling butane adsorption in MFI and MEL-type zeolites than the single-site model with variable q_{sat}.

The n-C_4 and i-C_4 adsorption isotherms measured for the membranes were fit well with the dual-site Langmuir model that assumed $q_{satC,n\text{-}C4} = 8$, $q_{satI,n\text{-}C4} = 2$, $q_{satI,i\text{-}C4} = 4$, and $q_{satC,i\text{-}C4} = 6$ molec./u.c. Figures 12–14 show that the adsorp-

tion equilibrium constants have the expected exponential dependence on temperature, and the heats and entropies of adsorption (Table 4) are within the ranges reported in the literature for MFI-type powders and estimated by simulations for MFI and MEL-type zeolites (Schenk et al., 2002; Vlugt et al., 1999). Adsorption measurements for butane isomers on MEL powders were not found in the literature.

Three of the four i-C_4 adsorption isotherms measured in the Al-ZSM-11 membrane (Figure 10) were measured with a feed total pressure of about 84 kPa and no total pressure drop across the membrane. The 406 K isotherm was measured with a feed total pressure of about 117 kPa and a total pressure drop across the membrane of about 33 kPa. The isotherm measurements were apparently not affected by the total pressure drop across the membrane, since the 406 K isotherm is between the 435 and 384 K isotherms and the adsorption equilibrium constants for all four temperatures lie on a straight line in the Arrhenius plots (Figures 13 and 14).

Membrane comparison

The heats and entropies of adsorption of both isomers measured in the Al-ZSM-5 membrane were almost the same as those measured on silicalite powder by Zhu et al. (2000) and fit with the dual-site Langmuir model. The Al-ZSM-5 adsorption properties were closest of the three membranes studied to the properties of the silicalite powder because silicalite and ZSM-5 have the same structure, and the Al-ZSM-5 membrane was less substituted (Si/Al = 600) than the B-ZSM-5 membrane (Si/B = 100).

MFI compared to MEL

The measured heats and entropies of adsorption for n-C_4 and for i-C_4 in the intersections were similar in the Al-ZSM-5 and Al-ZSM-11 membranes. They are also similar to the heats and entropies of adsorption of n-C_4 and i-C_4 calculated from simulated isotherms between 300 and 473 K on the all-silica forms of ZSM-5 and ZSM-11 (Schenk et al., 2002) (Table 4). The Al-ZSM-5 and Al-ZSM-11 membranes had Si/Al ratios of 600, so the properties of the adsorption sites are expected to be similar in the two membranes.

The notable difference between the adsorption properties of the two structures is that the i-C_4 coverages were higher in the MEL membrane than in the MFI membrane (Figures 9 and 10). Because the saturation coverages were the same in the two structures (4 molec./u.c. in the intersections and 6 molec./u.c. in the channels), the coverages were higher in MEL because the adsorption equilibrium constants, which are determined by the heat and entropy change upon adsorption, were higher. Although the thermodynamic properties have significant error, as shown by the standard deviations, the experimental error in the adsorption isotherm points is not high enough to account for the i-C_4 coverage differences in the two structures. Based on the standard deviation error estimates, the measured heats and entropies of i-C_4 adsorption in the intersections of the two structures are not significantly different, but the heat of adsorption was lower and the entropy changed less upon adsorption of i-C_4 in the *channels* of MEL than in MFI (Table 4). Molecular simulations of the all-silica forms of the two structures also showed that the i-C_4 heat and entropy changes upon adsorption in the channels were lower in MEL than in MFI, and that the structure did not significantly affect the adsorption properties of n-C_4 or i-C_4 in the intersections. Adsorption equilibrium constants, and thus the coverage at a given temperature and pressure, decrease with decreasing $|-\Delta H_{ads}|$ and increase with decreasing $|-\Delta S_{ads}|$. Because the thermodynamic adsorption properties of i-C_4 in the channels were both lower in MEL than in MFI, the difference in entropy change upon adsorption led to the higher coverages in MEL.

The lower heat and entropy of i-C_4 adsorption in MEL channels indicate that i-C_4 molecules are less constrained when adsorbed in the slightly more open and symmetrical channels in MEL than in the elliptical MFI pores. This difference in adsorption behavior helps explain the significantly higher mobility of i-C_4 in MEL than in MFI. Because molecules must adsorb in the channels at least temporarily to diffuse through the membranes, and i-C_4 adsorbs more easily (less entropy change upon adsorption) and less strongly (lower heat of adsorption) in the channels of MEL than of MFI, the i-C_4 diffusivity should be higher in MEL than in MFI. Because the pore mouths of the channels are the most constrained areas (smallest openings) and the diameter of i-C_4 is close to the size of the pore mouths but the diameter of n-C_4 is smaller, i-C_4 must overcome a larger energy barrier to diffuse than n-C_4, so differences in the pore mouths affect i-C_4 diffusion more than n-C_4 diffusion. Thus, the diffusion and adsorption properties of n-C_4 are similar in the two structures because the n-C_4 molecules are small enough not to be significantly affected by small changes in the pore size. Similarly, the adsorption properties of i-C_4 in the intersections of the two structures are comparable because the intersections are larger than the channels and small changes in their size or configuration do not affect i-C_4 adsorption.

Another interesting difference between the adsorption properties of n-C_4 and i-C_4 in the MEL and MFI structures is that the channel and intersection adsorption equilibrium constants are more similar in MEL than in MFI. As noted earlier, the distinction between channel and intersection sites for n-C_4 adsorption was also less clear in MEL than in MFI for simulated isotherms.

B-ZSM-5 compared to Al-ZSM-5

As in the Al-ZSM-11 membrane, the n-C_4 adsorption properties were similar and the i-C_4 coverages were higher in the B-ZSM-5 than in the Al-ZSM-5 membrane (Figures 9 and 11). Changes in heat and entropy upon i-C_4 adsorption were similar in the intersections and lower in the channels of the Al-ZSM-11 than in the channels of the Al-ZSM-5 membrane. The higher coverages in Al-ZSM-11 were caused by the lower entropy change upon adsorption in the channels. In contrast, the estimated heat and entropy changes upon i-C_4 adsorption were similar in the channels and higher in the intersections of the more substituted B-ZSM-5 membrane than of the Al-ZSM-5 membrane (Table 4). Thus, the higher heat of adsorption in the intersections led to the higher i-C_4 coverages in the B-ZSM-5 membrane. The heat of adsorption is a lumped property over all adsorption sites, so the amount of substitution and the difference in the sites contribute to the difference in $-\Delta H_{ads}$. The Brønsted acidity of B- or Al-substituted sites is higher than that of Si sites in the MFI framework (Chatterjee and Chandra,

1997; Yuan et al., 2002), and the energy of adsorption is higher on substituted sites as well (Yuan et al., 2002). The heats of adsorption of the butane isomers on the ZSM-5 zeolites are higher than those measured and simulated in silicalite-1. The Bronsted acidity of B-substituted sites is lower than that of Al-substituted sites (Chatterjee and Chandra, 1997; Yuan et al., 2002), so heats of adsorption on B-ZSM-5 should be lower than those on Al-ZSM-5 with the same substitution ratio. Six times more silicon atoms were substituted with boron atoms in the B-ZSM-5 membrane than with Al atoms in the Al-ZSM-5 membrane, which could explain why the i-C_4 heat of adsorption was higher in the B-ZSM-5 membrane. The heat and entropy of i-C_4 adsorption in the channels are similar in the B-ZSM-5 and Al-ZSM-5 membranes, perhaps because the framework substitution occurs preferentially at the intersection sites (Chatterjee and Chandra, 1997).

The fact that substitution mainly takes place in the intersections may also explain why the n-C_4 adsorption and diffusion properties were essentially the same in the Al-ZSM-5 and B-ZSM-5 membranes. The first eight n-C_4 molecules per unit cell adsorbing in ZSM-5 adsorb in the channels, which are essentially the same in Al-ZSM-5 and B-ZSM-5 zeolites. At the lower temperatures, the n-C_4 coverages were slightly higher in the B-ZSM-5 membrane than in the Al-ZSM-5 membrane (Figures 6 and 8), which was why the n-C_4 adsorption properties in the intersections of the B-ZSM-5 membrane could be measured. This suggests that n-C_4 adsorbed more strongly in the intersections of the B-ZSM-5 than in the Al-ZSM-5 membrane. Indeed, the n-C_4 heat and entropy of adsorption were higher in the intersections of the B-ZSM-5 membrane than in the channels of any of the structures and were higher than any of the heats and entropies of adsorption reported in the literature for silicalite. However, higher coverage isotherms would have to be measured to quantify the heat and entropy of n-C_4 adsorption in the intersections of the Al-ZSM-5 membrane to test this explanation.

We suggested in the previous section that the i-C_4 diffusivities were higher in MEL because i-C_4 adsorbed less strongly in MEL than in MFI channels, so the molecules were less constrained and therefore more mobile. Similarly, the i-C_4 molecules adsorbed more strongly and their diffusivities were slightly lower in the B-ZSM-5 than in the Al-ZSM-5 membrane.

Transient permeation

Model Fits. The transient responses generated from the model would better fit the data by including the coverage dependency of the Maxwell–Stefan diffusivity. The model changes the diffusivity from the steady-state value at one feed concentration to that at another by changing $Đ_{MS}$ as the coverage in the middle of the membrane changes from one steady-state value to another. Thus, the diffusivity was the same at every point in the membrane for each time step, although it should be a function of the coverage at each position. The transient model fits were best for the B-ZSM-5 membrane because the diffusivity changed least with coverage in B-ZSM-5 and the model assumes a constant $Đ_{MS}$ for each step.

Initial Transients. The overshoots and undershoots in the i-C_4 transient fluxes after feed step changes (Figures 21–23) were apparently caused by the total pressure drop between the feed and permeate sides of the membranes because the transient i-C_4 fluxes exhibited these extrema only in the Al-ZSM-11 membrane when a total pressure difference was applied across the membrane (Figure 23). Because the n-C_4 fluxes (and light gas fluxes reported previously (Gardner et al., 2002a)) increased and decreased monotonically after feed concentration changes, even with an absolute pressure drop across the membrane, the extrema in the i-C_4 fluxes are likely related to membrane properties rather than being experimental artifacts. Because the i-C_4 fluxes were much lower than the n-C_4 and light gas fluxes, and were therefore potentially more sensitive to small perturbations in the system, other measurements were made to verify that the initial transients did not result from experimental artifacts. The total pressures on the feed, retentate, and permeate sides and in the mass spectrometer chamber did not change during feed step changes. Also, the permeate flux did not change when the feed to the membrane was switched back and forth between two streams with the same i-C_4 concentration in helium. The model did not predict overshoots or undershoots (Figures 18 and 20), so these phenomena are probably not attributable to the single component permeation through the zeolite pores.

Transport through polycrystalline membranes can occur through both intracrystalline (zeolite) and intercrystalline (non-zeolite) pores, in series and in parallel. Attempts have been made to characterize the parallel non-zeolite pores by the initial transient permeate responses after step changes in the feed to empty membranes (Burggraaf et al., 1998; Gardner et al., 2002b), by permporosimetry (Deckman et al., 2001; Hedlund et al., 2002), confocal microscopy (Bonilla et al., 2001a,b; Nair et al., 2001; Nelson et al., 2001), modeling steady-state fluxes including contributions from Knudsen diffusion and viscous flow (Poshusta et al., 1999; van de Graaf et al., 1999), and the permeation behavior after partial calcination (Lin et al., 1998; van de Graaf et al., 1999). The initial transient permeate response through ZSM-5 membranes at 383 K to a feed step change from 0 to 6 kPa of i-C_4 showed a two-step approach to steady state, from which we concluded that about 4% of the i-C_4 flow was through parallel non-zeolite pores (Gardner et al., 2002b). The transient flux of n-C_4 through an initially empty membrane approached steady state in a single step, indicating that less than 0.01% of its flow (the detection limit) was through pores with a significantly shorter breakthrough time than the zeolite pores. Because i-C_4 diffused more slowly than n-C_4 through the zeolite pores, a relatively larger fraction of i-C_4 flow was through non-zeolite pores. The initial transient extrema may be caused by flow through parallel non-zeolite pores. Thus only the i-C_4 flux exhibits this behavior because it has a measurable fraction of its flow through parallel non-zeolite pores; the fraction of n-C_4 flow through the parallel pathways that are affected by the total pressure drop is too low for a change in its flow to be noticeable.

The permeate flow rate was monitored during a switch from 100 to 5% i-C_4 in helium (117 kPa feed pressure, 84 kPa permeate pressure) feed to the B-ZSM-5 membrane at 474 K (Figure 26). When the feed was switched, the mass spectrometer signal for i-C_4 increased through a maximum at about 0.5 min and then decreased as the zeolite pore flow decreased. The i-C_4 flux increase of about 8% equates to a permeate flow rate increase of about 0.01 cm^3/min (standard temperature and pressure), which was not measurable with the digital flowme-

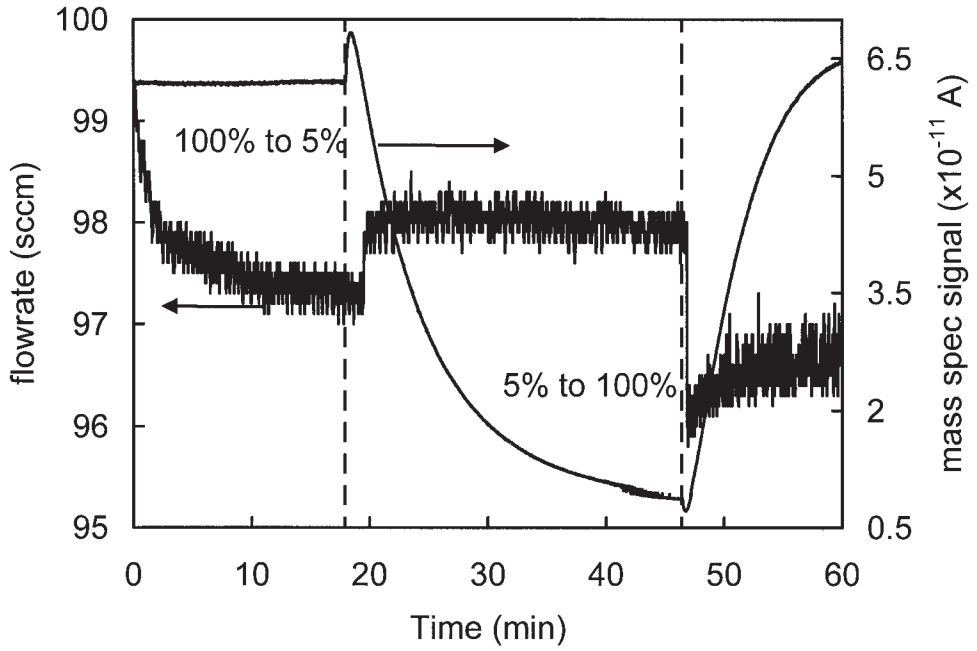

Figure 26. Initial i-C_4 transient permeate responses and total permeate flow rate after feed step changes from 100 to 5% and from 5 to 100% i-C_4 in helium at 474 K through a B-ZSM-5 membrane.

ter. Approximately 1 min after the maximum in i-C_4 flux, the total permeate flow rate jumped from about 97.3 to about 98 cm^3/min (standard temperature and pressure).

Similarly, when the i-C_4 feed concentration increased from 5 to 100%, the i-C_4 signal decreased through a minimum at about 0.34 min and then increased as the zeolite pore flow increased. A few seconds after the minimum, the total permeate flow rate dropped from 98 to 96 cm^3/min (standard temperature and pressure), presumably as the non-zeolite pores emptied of helium. The time required for the total permeate flow rate to change is proportional to the amount of helium in the non-zeolite pores before the change. The initial transients could potentially be used to measure the flow through parallel non-zeolite pores.

Summary

Dual-site Langmuir adsorption isotherms of butane isomers in ZSM-11 and ZSM-5 membranes were measured by a transient permeation method. The effects of diffusion differences and driving force ratios were separately quantified. More i-C_4 adsorbed in the Al-ZSM-11 than in the Al-ZSM-5 membrane because the entropy changed less upon i-C_4 adsorption in the slightly larger and more rounded ZSM-11 channels. The ideal selectivities were higher in the ZSM-5 membranes than in the ZSM-11 membrane because the mobility of the bulkier branched isomer was higher in the rounded ZSM-11 pores, although the mobility of the linear isomer was not. More i-C_4 adsorbed in the more substituted B-ZSM-5 than in the Al-ZSM-5 membrane because the heat of adsorption in the intersections (where framework substitution preferentially occurs) was higher in the more substituted membrane. The n-C_4/i-C_4 ideal selectivity in the B-ZSM-5 membrane increased between 449 and 474 K because the ratio of adsorption driving forces increased more than the ratio of diffusivities decreased with temperature. Because of the support resistance, the permeate boundary coverage was raised, and this lowered the ideal selectivities in all membranes compared to what could have been attained with zero permeate coverage. Undershoots and overshoots in the initial transient permeate response to i-C_4 feed concentration step increases and decreases, respectively, were attributed to pressure driven flow through parallel non-zeolite pores.

Acknowledgments

The authors thank Professors B. Smit and R. Krishna and their research groups at University of Amsterdam, especially Merijn Schenk, for providing simulation data and for useful discussions. We gratefully acknowledge support by the National Science Foundation Grant CTS-99 08796. T.Q.G. also gratefully acknowledges support from a Department of Education Government Assistance for Areas of National Need (GAANN) fellowship.

Notation

A = area of zeolite membrane available for permeation, m^2
b = adsorption equilibrium constant, kPa^{-1}
δ = membrane thickness, μm
$Đ_{MS}$ = Maxwell–Stefan diffusivity, m^2/s
Ea = activation energy for diffusion, kJ/mol
$-\Delta H_{ads}$ = heat of adsorption, kJ/mol
J_{in} = flux into the membrane at feed side, mol/m^2 s
J_{out} = flux out of the membrane at permeate side, mol/m^2 s
P = pressure, kPa
Π = permeance, mol/m^{2}s kPa
q = coverage, molecules/unit cell
q_{sat} = saturation coverage, molecules/unit cell
Q_c = total moles in membrane at steady state by coverage profile, mol
Q_t = total moles in membrane at steady state by transient flux, mol
ρ = zeolite density, unit cells/m^3
θ = fractional coverage
t_{SS} = time for flux to reach steady state, s

Literature Cited

Bai, C., M.-D. Jia, J. L. Falconer, and R. D. Noble, "Preparation and Separation Properties of Silicalite Composite Membranes," *J. Membr. Sci.*, **105**, 79 (1995).

Bakker, W. J. W., F. Kapteijn, J. Poppe, and J. A. Moulijn, "Permeation Characteristics of a Metal-Supported Silicalite-1 Zeolite Membrane," *J. Membr. Sci.*, **117**, 57 (1996).

Bein, T., "Synthesis and Applications of Molecular Sieve Layers and Membranes," *Chem. Mater.*, **8**, 1636 (1996).

Bonilla, G., M. Tsapatsis, D. G. Vlachos, and G. Xomeritakis, "Fluorescence Confocal Optical Microscopy Imaging of the Grain Boundary Structure of Zeolite MFI Membranes Made by Secondary (Seeded) Growth," *J. Membr. Sci.*, **182**, 103 (2001).

Bonilla, G., D. G. Vlachos, and M. Tsapatsis, "Simulations and Experiments on the Growth and Microstructure of Zeolite MFI Films and Membranes Made by Secondary Growth," *Micro. Meso. Mater.*, **42**, 191 (2001).

Burggraaf, A. J., "Single Gas Permeation of Thin Zeolite (MFI) Membranes: Theory and Analysis of Experimental Observations," *J. Membr. Sci.*, **155**, 45 (1999).

Burggraaf, A. J., Z. A. E. P. Vroon, K. Keizer, and H. Verweij, "Permeation of Single Gases in Thin Zeolite MFI Membranes," *J. Membr. Sci.*, **144**, 77 (1998).

Chatterjee, A., and A. K. Chandra, "Fe and B Substitution in ZSM-5 Zeolites: A Quantum-Mechanical Study," *J. Mol. Catal. A: Chemical*, **119**, 51 (1997).

Davis, M. E., and R. F. Lobo, "Zeolite and Molecular Sieve Synthesis," *Chem. Mater.*, **4**, 756 (1992).

Deckman, H. W., D. M. Cox, A. J. Bons, B. Carstensen, R. R. Chance, E. W. Corcoran, W. De Gijnst, J. A. McHenry, J. J. Reinoso, R. B. Saunders, and P. J. Tindall, "Characterization of Zeolite Membrane Quality and Structure," Proc. of IWZMM Conference, July 1–4, Purmerend, The Netherlands, p. 9 (2001).

den Exter, M. J., J. C. Jansen, J. M. van de Graaf, F. Kapteijn, J. A. Moulijn, and H. van Bekkum, "Zeolite-Based Membranes Preparation, Performance and Prospects," *Stud. Surf. Sci. Catal.: Rec. Adv. New Horizons in Zeolite Sci. and Technol.*, **102**, 413 (1996).

Gardner, T. Q., J. L. Falconer, R. D. Noble, and M. Zieverink, "Analysis of Transient Permeation Fluxes into and out of Membranes for Adsorption Measurements," *Chem. Eng. Sci.*, **58**, 2103 (2003).

Gardner, T. Q., A. I. Flores, R. D. Noble, and J. L. Falconer, "Transient Measurement of Adsorption and Diffusion in H-ZSM-5 Membranes," *AIChE J.*, **48**, 1155 (2002).

Gardner, T. Q., J. B. Lee, R. D. Noble, and J. L. Falconer, "Adsorption and Diffusion Properties of Butanes in ZSM-5 Zeolite Membranes," *Ind. Eng. Chem. Res.*, **41**, 4094 (2002).

Goodbody, S. J., K. Watanabe, D. MacGowan, J. P. R. B. Walton, and N. Quirke, "Molecular Simulation of Methane and Butane in Silicalite," *J. Chem. Soc. Faraday Trans.*, **87**, 1951 (1991).

Gora, L., N. Nishiyama, J. C. Jansen, F. Kapteijn, V. Teplyakov, and Th. Maschmeyer, "Highly Reproducible High-Flux Silicalite-1 Membranes: Optimization of Silicalite-1 Membrane Preparation," *Sep. Purif. Technol.*, **22–23**, 223 (2001).

Hedlund, J., B. Schoeman, and J. Sterte, "Ultrathin Oriented Zeolite LTA Films," *Chem. Commun.*, **13**, 1193 (1997).

Hedlund, J., J. Sterte, M. Anthonis, A.-J. Bons, B. Carstensen, N. Corcoran, D. Cox, H. Deckman, W. De Gijnst, P.-P. de Moor, F. Lai, J. McHenry, W. Mortier, J. Reinoso, and J. Peeters, "High-Flux MFI Membranes," *Micro. Meso. Mater.*, **52**, 179 (2002).

Jia, M.-D., B. Chen, R. D. Noble, and J. L. Falconer, "Ceramic-Zeolite Composite Membranes and Their Application for Separation of Vapor/Gas Mixtures," *J. Membr. Sci.*, **90**, 1 (1994).

Kapteijn, F., W. J. W. Bakker, J. M. van de Graaf, G. Zheng, J. Poppe, and J. A. Moulijn, "Permeation and Separation Behavior of a Silicalite-1 Membrane," *Catal. Today*, **25**, 213 (1995).

Kapteijn, F., W. J. W. Bakker, G. Zheng, J. Poppe, and J. A. Moulijn, "Permeation and Separation of Light Hydrocarbons through a Silicalite-1 Membrane—Application of the Generalized Maxwell–Stefan Equations," *Chem. Eng. J.*, **57**, 145 (1995).

Kapteijn, F., J. A. Moulijn, and R. Krishna, "The Generalized Maxwell–Stefan Model for Diffusion in Zeolites: Sorbate Molecules with Different Saturation Loadings," *Chem. Eng. Sci.*, **55**, 2923 (2000).

Krishna, R., and L. J. P. van den Broeke, "The Maxwell–Stefan Description of Mass Transport across Zeolite Membranes," *Chem. Eng. J.*, **57**, 155 (1995).

Krishna, R., T. J. H. Vlugt, and B. Smit, "Influence of Isotherm Inflection on Diffusion in Silicalite," *Chem. Eng. Sci.*, **54**, 1751 (1999).

Kusakabe, K., T. Kuroda, and S. Morooka, "Separation of Carbon Dioxide from Nitrogen Using Ion-Exchanged Faujasite-Type Zeolite Membranes Formed on Porous Support Tubes," *J. Membr. Sci.*, **148**, 13 (1998).

Kusakabe, K., T. Kuroda, K. Uchino, Y. Hasegawa, and S. Morooka, "Gas Permeation Properties of Ion-Exchanged Faujasite-Type Zeolite Membranes," *AIChE J.*, **45**, 1220 (1999).

Li, S., V. A. Tuan, J. L. Falconer, and R. D. Noble, "Separation of 1,3-Propanediol from Glycerol and Glucose Using an X-Type Zeolite Membrane," *Ind. Eng. Chem. Res.*, **40**, 1952 (2001).

Li, S. G., V. A. Tuan, R. D. Noble, and J. L. Falconer, "ZSM-11 Membranes: Characterization and Pervaporation Performance," *AIChE J.*, **48**, 269 (2002).

Li, S. G., V. A. Tuan, R. D. Noble, and J. L. Falconer, "Properties and Separation Performance of Ge-ZSM-5 Membranes," *Micro. Meso. Mater.*, **58**, 137 (2003).

Lin, X., J. L. Falconer, and R. D. Noble, "Parallel Pathways for Transport in ZSM-5 Zeolite Membranes," *Chem. Mater.*, **10**, 3716 (1998).

Maesen, T., M. Schenk, T. Vlugt, and B. Smit, "Differences between MFI and MEL-Type Zeolites in Paraffin Hydrocracking," *J. Catal.*, **203**, 281 (2001).

Matsukata, M., and E. Kikuchi, "Zeolitic Membranes: Synthesis, Properties, and Prospects," *Bull. Chem. Soc. Jpn.*, **70**, 2341 (1997).

Matsukata, M., N. Nishiyama, and K. Ueyama, "Synthesis of Zeolites under Vapor Atmosphere—Effect of Synthetic Conditions on Zeolite Structure," *Micro. Mater.*, **1**, 219 (1993).

Matsukata, M., N. Nishiyama, and K. Ueyama, "Crystallization of FER and MFI Zeolites by a Vapor-Phase Transport Method," *Micro. Mater.*, **7**, 109 (1996).

Meier, W. M., and D. H. Olson, *Atlas of Zeolite Structure Types*, 3rd Edition, Butterworth-Heinemann, London (1992).

Millot, B., A. Methivier, H. Jobic, H. Moueddeb, and M. Bee, "Diffusion of Isobutane in ZSM-5 Zeolite: A Comparison of Quasi-Elastic Neutron Scattering and Supported Membrane Results," *J. Phys. Chem. B*, **103**, 1096 (1999).

Nair, S., Z. Lai, V. Nikolakis, G. Xomeritaxis, G. Bonilla, and M. Tsapatsis, "Separation of Close-Boiling Hydrocarbon Mixtures by MFI and FAU Membranes Made by Secondary Growth," *Micro. Meso. Mater.*, **48**, 219 (2001).

Nelson, P. H., M. Tsapatsis, and S. M. Auerbach, "Modeling Permeation through Anisotropic Zeolite Membranes with Nanoscopic Defects," *J. Membr. Sci.*, **184**, 245 (2001).

Nishiyama, N., T. Matsufuji, K. Ueyama, and M. Matsukata, "FER Membrane Synthesized by a Vapor-Phase Transport Method: Its Structure and Separation Characteristics," *Micro. Mater.*, **12**, 293 (1997).

Noble, R. D., and J. L. Falconer, "Silicalite-1 Zeolite Composite Membranes," *Catal. Today*, **25**, 209 (1995).

Poshusta, J. C., J. L. Falconer, and R. D. Noble, "Temperature and Pressure Effects on CO_2 and CH_4 Permeation through MFI Zeolite Membranes," *J. Membr. Sci.*, **160**, 115 (1999).

Poshusta, J.C., V. A. Tuan, E. A. Pape, R. D. Noble, and J. L. Falconer, "Separation of Light Gas Mixtures Using SAPO-34 Membranes," *AIChE J.*, **46**, 779 (2000).

Schenk, M., B. Smit, and R. Krishna, Unpublished results (2002).

Tuan, V.A., J. L. Falconer, and R. D. Noble, "Alkali-Free ZSM-5 Membranes: Preparation Conditions and Separation Performance," *Ind. Eng. Chem. Res.*, **38**, 3635 (1999).

Tuan, V.A., J. L. Falconer, and R. D. Noble, "Isomorphous Substitution of Al, Fe, B, and Ge into MFI-Zeolite Membranes," *Micro. Meso. Mater.*, **41**, 269 (2000a).

Tuan, V.A., J. L. Falconer, and R. D. Noble, "Boron Substituted ZSM-5 Membranes: Preparation and Separation Performance," *AIChE J.*, **46**, 1201 (2000b).

Tuan, V. A., S. Li, J. L. Falconer, and R. D. Noble, "In-Situ Crystallization of Beta Zeolite Membranes and Their Permeation and Separation Properties," *Chem. Mater.*, **14**, 489 (2002).

Tuan, V. A., S. G. Li, R. D. Noble, and J. L. Falconer, "Preparation and Pervaporation Properties of a MEL-Type Zeolite Membrane," *Chem. Commun.*, **6**, 583 (2001).

van de Graaf, J. M., F. Kapteijn, and J. A. Moulijn, "Modeling Permeation

of Binary Mixtures through Zeolite Membranes," *AIChE J.*, **45**, 497 (1999a).
van de Graaf, J. M., F. Kapteijn, and J. A. Moulijn, "Permeation of Weakly Adsorbing Components through a Silicalite-1 Membrane," *Chem. Eng. Sci.*, **54**, 1081 (1999b).
van den Broeke, L. J. P., "The Maxwell–Stefan Theory for Micropore Diffusion," PhD Thesis, Universiteit van Amsterdam, The Netherlands (1994).
van Koningsveld, H., and J. C. Jansen, "Single Crystal Structure Analysis of Zeolite H-ZSM-5 Loaded with Naphthalene," *Micro. Mater.*, **6**, 159 (1996).
Vlugt, T. J. H., R. Krishna, and B. Smit, "Molecular Simulations of Adsorption Isotherms for Linear and Branched Alkanes and Their Mixtures in Silicalite," *J. Phys. Chem. B*, **103**, 1102 (1999).
Vroon, Z. A. E. P., "Synthesis and Transport Studies of Thin Ceramic Supported Zeolite (MFI) Membranes," PhD Thesis, Universiteit van Twente, The Netherlands (1995).
Vroon, Z. A. E. P., K. Keizer, A. J. Burggraaf, and H. Verweij, "Preparation and Characterization of Thin Zeolite MFI Membranes on Porous Supports," *J. Membr. Sci.*, **144**, 65 (1998).
Xomeritakis, G., A. Gouzmis, S. Nair, T. Okubo, M. He, R. M. Overney, and M. Tsapatsis, "Growth, Microstructure, and Permeation Properties of Supported Zeolite (MFI) Films and Membranes Prepared by Secondary Growth," *Chem. Eng. Sci.*, **54**, 3521 (1999).
Yan, Y., M. E. Davis, and G. R. Gavalas, "Preparation of Zeolite ZSM-5 Membranes by In-Situ Crystallization on Porous α-Al_2O_3," *Ind. Eng. Chem. Res.*, **34**, 1652 (1995).
Yuan, S. P., J. G. Wang, Y. W. Li, and S. Y. Peng, "Theoretical Studies on the Properties of Acid Site in Isomorphously Substituted ZSM-5," *J. Mol. Catal. A: Chemical*, **178**, 267 (2002).
Zhu, W., F. Kapteijn, and J. A. Moulijn, "Adsorption of Light Alkanes on Silicalite-1: Reconciliation of Experimental Data and Molecular Simulations," *Phys. Chem. Chem. Phys.*, **2**, 1989 (2000).
Zhu, W., J. M. van de Graaf, L. J. P. van den Broeke, F. Kapteijn, and J. A. Moulijn, "TEOM: A Unique Technique for Measuring Adsorption Properties. Light Alkanes in Silicalite-1," *Ind. Eng. Chem. Res.*, **37**, 1934 (1998).

Manuscript received Aug. 19, 2003, and revision received Feb. 26, 2004.